

## RESEARCH ARTICLE

# PPP4C facilitates homologous recombination DNA repair by dephosphorylating PLK1 during early embryo development

Ming-Zhe Dong<sup>1,2</sup>, Ying-Chun Ouyang<sup>1</sup>, Shi-Cai Gao<sup>1,2</sup>, Xue-Shan Ma<sup>1</sup>, Yi Hou<sup>1</sup>, Heide Schatten<sup>3</sup>, Zhen-Bo Wang<sup>1,2,\*</sup> and Qing-Yuan Sun<sup>4,\*</sup>

**ABSTRACT**

Mammalian early embryo cells have complex DNA repair mechanisms to maintain genomic integrity, and homologous recombination (HR) plays the main role in response to double-strand DNA breaks (DSBs) in these cells. Polo-like kinase 1 (PLK1) participates in the HR process and its overexpression has been shown to occur in a variety of human cancers. Nevertheless, the regulatory mechanism of PLK1 remains poorly understood, especially during the S and G2 phase. Here, we show that protein phosphatase 4 catalytic subunit (PPP4C) deletion causes severe female subfertility due to accumulation of DNA damage in oocytes and early embryos. PPP4C dephosphorylated PLK1 at the S137 site, negatively regulating its activity in the DSB response in early embryonic cells. Depletion of PPP4C induced sustained activity of PLK1 when cells exhibited DNA lesions that inhibited CHK2 and upregulated the activation of CDK1, resulting in inefficient loading of the essential HR factor RAD51. On the other hand, when inhibiting PLK1 in the S phase, DNA end resection was restricted. These results demonstrate that PPP4C orchestrates the switch between high-PLK1 and low-PLK1 periods, which couple the checkpoint to HR.

**KEY WORDS:** Embryo, PPP4C, DNA damage, PLK1, CDK1, Homologous recombination

**INTRODUCTION**

Homologous recombination (HR), which serves to eliminate deleterious lesions, such as double-strand DNA breaks (DSBs) and interstrand crosslinks, from chromosomes, is indispensable for maintenance of genome integrity and protection against cancers in humans (San Filippo et al., 2008). Two important steps of HR include: DSB end resection, which is induced by exo- and endonuclease, such as CtIP, Mre11 and EXO1 (Chapman et al., 2012; Shibata et al., 2014; Chanut et al., 2016), following the formation of RPA-coated 3' single strand DNA (ssDNA) ends; and single-strand invasion, which involves displacement of RPA from the ssDNA and assembly of RAD51 filaments mediated by BRCA2 (Ciccio and Elledge, 2010), following the formation of D-loop structures and DNA synthesis.


During the transition of the two steps, numerous kinases and phosphatases are coordinated in the regulation of the progression. PLK1, a highly conserved serine/threonine kinase, is typically overexpressed in cancer cell lines and is considered to be a potential target for antisense tumor therapy (Elez et al., 2000; Liu et al., 2017). Paradoxically, PLK1 is recruited, stimulating DNA end resection and promoting HR by suppressing the canonical DNA double-strand break ubiquitylation response at broken forks (Nakamura et al., 2021); however, PLK1-mediated phosphorylation of CtIP promotes error-prone microhomology-mediated end-joining (MMEJ), which fails to initiate extended end resection and suppresses HR (Wang et al., 2018). On the other hand, PLK1 phosphorylates the essential RAD51 recombinase at serine 14 during the cell cycle, which facilitates its recruitment to damaged sites and promotes HR-mediated repair (Yata et al., 2012; Peng et al., 2021); however, PLK1 also inhibits the checkpoint kinase CHK2 by inactivating its FHA domain, which dismantles the DNA damage checkpoint and is detrimental to DNA damage repair (van Vugt et al., 2010). Furthermore, PLK1 upregulates the activation of CDK1 by suppression of Wee1 and Myt1 (van Vugt et al., 2004; Inoue and Sagata, 2005), and activation of CDC25 (Qian et al., 2001; Lobjois et al., 2009; Tang et al., 2020) in both normal condition and after DNA damage-induced G2/M arrest. In human cells, DSB end resection requires the regulation of CDKs (Huertas and Jackson, 2009), but it must be inactivated after DNA end resection, which allows Rad51 and BRCA2 to interact and use the RPA-coated ssDNA to initiate single strand invasion (Esashi et al., 2005; Jazayeri et al., 2006; Buisson et al., 2017). Remi et al. provided a model in which HR is a biphasic process requiring both high-CDK and low-CDK periods (Buisson et al., 2017), but whether the activity of PLK1 also changes dynamically during HR is not known; if it does, what regulates the inactivation of PLK1 in checkpoint response?

In mammalian species, two conserved sites [Ser137 (S137) and Thr210 (T210)] of phosphorylation are associated with the activation of PLK1. Although it had been reported that PLK1 could be inhibited in response to DNA damage (Smits et al., 2000; Tang et al., 2006; Jang et al., 2007), in which CHK1 or PP2A might be involved in its regulation, how the two conserved sites of PLK1 may be dephosphorylated during HR has not yet been determined.

In 2008, Kazuhito and colleagues found that PPP4C could negatively regulate Cdk1 activity in mouse embryonic fibroblast (MEF) cells (Toyo-oka et al., 2008). Although they demonstrated the function of PP4C in microtubule (MT) organization, they did not investigate its function in the DNA damage response (DDR) or the cause of an unscheduled activation of Cdk1. Other studies before and since showed the PPP4 involvement in the activity of the critical DNA repair factors H2AX, RPA2, KAP-1 and 53BP1 (Keogh et al., 2006; Chowdhury et al., 2008; Nakada et al., 2008; Lee et al., 2010, 2012, 2014; Isono et al., 2017), but the physiological role of PPP4 in

<sup>1</sup>State Key Laboratory of Stem Cell and Reproductive Biology, Institute of Zoology, Chinese Academy of Sciences, Beijing 100101, China. <sup>2</sup>University of Chinese Academy of Sciences, Beijing 100101, China. <sup>3</sup>Department of Veterinary Pathobiology, University of Missouri, Columbia, MO 65211, USA. <sup>4</sup>Fertility Preservation Lab, Guangdong-Hong Kong Metabolism & Reproduction Joint Laboratory, Reproductive Medicine Center, Guangdong Second Provincial General Hospital, Guangzhou 510317, China.

\*Authors for correspondence (sunqy@gd2h.org.cn; wangzb@ioz.ac.cn)

 M.-Z.D., 0000-0001-6562-3987; X.-S.M., 0000-0003-0801-7061; Q.-Y.S., 0000-0002-0148-2414

Handling Editor: Haruhiko Koseki

Received 11 November 2021; Accepted 24 April 2022

mammalian species, especially its relationship with CDK1, needs to be systematically identified.

The two major pathways for DSB repair are thought to act as follows: non-homologous end joining (NHEJ) is used primarily in the G1 phase of the cell cycle, while HR is used primarily in the S and G2 phase, following replication of the genome (Symington and Gautier, 2011). However, unlike somatic cells, early developing embryos have an extremely short G1 phase (Artus and Cohen-Tannoudji, 2008) and HR is the main pathway responsible for the promotion of DSB repair (Bohrer et al., 2018), including in mammalian zygotes (Smirnov et al., 2020). A violation of genomic integrity during the embryonic period often leads to death (Khokhlova et al., 2020), corresponding disease and pregnancy loss. According to the features of DNA repair, early developing embryos provide a suitable model to study the HR process. On the other hand, oocytes in growing follicles show higher resistance to DNA damage than somatic cells (Marangos and Carroll, 2012; Nguyen et al., 2019; Gebel et al., 2020), which makes their use a new avenue for researching DNA damage response in early embryos by specific knockout of maternal factors. There have been studies showing that maternal depletion of DDR factors only impacts DDR in embryos without having any detrimental effect on oocyte maturation (Xu et al., 2015; Huang et al., 2019; Zhang et al., 2019).

In this study, we investigated the function of PPP4C in early embryo cells using a conditional knockout approach. Initially, we found that PPP4C-deficient females were subfertile due to DDR defects. Furthermore, we determined that CDK1 was unusually activated after DNA end resection, after which CDK1 should be deactivated. Finally, we showed that PPP4C regulated CDK1 by dephosphorylating PLK1 at the S137 site during HR.

## RESULTS

### Generation of *Ppp4c* conditional knockout mouse line

To study the functions of PPP4C during oogenesis and early embryo development, its expression was first analyzed by immunoblotting extracts from germinal vesicle (GV) oocytes to two-cell stage embryos using an antibody directed against mouse PPP4C (Fig. S1A). PPP4C was expressed throughout the oocyte meiotic maturation process and embryo development. The subcellular localization of PPP4C in mouse oocytes was further investigated by immunofluorescence staining (Fig. S1B,C). PPP4C was distributed in both nuclei and cytoplasm during oocyte meiotic maturation and during embryo development without specific localization. We constructed a conditional knockout C57BL/6J background mouse line of *Ppp4c* by CRISPR/Cas9-Mediated Genome Engineering, in which exon 3 of *Ppp4c* was flanked by LoxP sites (Fig. 1A). A total of 25 pups were born from 150 embryos transferred into foster mothers (17% live-birth rate). The PCR examination of each pup indicated that nine mice might carry the *Ppp4c* floxed allele, and five out of nine mice were picked out for sequencing, which indicated that all of the five mice carried the *Ppp4c* floxed allele (data not shown). *Ppp4c<sup>fl/fl</sup>* mice were crossed with transgenic mice expressing the Zp3 promoter-mediated Cre recombinase to generate *Ppp4c<sup>fl/fl</sup>; Zp3-Cre* male mice. *Ppp4c<sup>fl/fl</sup>; Zp3-Cre* male mice were then crossed with *Ppp4c<sup>fl/fl</sup>* female mice to generate *Ppp4c<sup>fl/fl</sup>* female mice (hereafter called wild type) as controls and *Ppp4c<sup>fl/fl</sup>; Zp3-Cre* female mice (hereafter called Zko) in which *Ppp4c* was specifically deleted in oocytes. The three *Ppp4c* alleles (flox, wild and an exon 3-deleted allele named  $\Delta$ ) were genotyped with PCR (Fig. 1B). By mRNA analysis and western blot, we confirmed that expression of *Ppp4c* gene in germinal vesicle oocytes from Zko females was absent (Fig. S2A, Fig. 1C).

### PPP4C is crucial for female fertility but is not essential for oocyte meiotic maturation

To investigate the effect of oocyte-specific knockout of PPP4C on female fertility, a breeding assay was carried out by mating wild-type or Zko female mice as they were 6 weeks old with wild-type C57BL/6J background males of proven fertility for 6 months. We checked daily for counting the cumulative total number of litters and pups per month (Table S1). As shown in Fig. 1D, Zko female mice were severely subfertile and gave birth to about 60% fewer pups than wild-type mice. To explore the reason for subfertility, natural ovulations of the two groups were assessed first. However, the number of eggs was not significantly different between mutant mice and the control (Fig. 1E,  $8.33 \pm 0.12$  versus  $7.69 \pm 0.17$ ,  $P > 0.05$ ). Furthermore, we compared the oocyte meiotic maturation progression in Zko mice with that in wild-type mice. The GV oocytes were employed for culture *in vitro* to observe the major events during the meiotic maturation process. Indeed, the absence of PPP4C seemed to have no influence on the oocyte meiotic maturation rate because there was no significant difference in PBE rates between the two groups (Fig. S2B,  $71.7 \pm 7.1\%$  versus  $61.7 \pm 4.8\%$ , respectively). Further analysis of spindle organization (Fig. S2C) and chromosome segregation (Fig. S2D) in the oocyte M II stage showed no significant difference between wild-type and the Zko group. Therefore, PPP4C might be dispensable for oocyte meiotic resumption and completion of the first meiosis.

### Loss of PPP4C leads to defective early embryonic development

To find the causes of female sub-fertility in Zko, we extended our observation to mouse embryo development. Embryos from wild-type and Zko females were collected at embryonic day (E) 0.5 and cultured *in vitro* to develop into the next cleavage stage. The zygotes from Zko female mice had extruded the second polar bodies and showed two visible pronuclei (Fig. 2A). However, only  $27.9 \pm 6.8\%$  embryos that were collected from Zko female mice could progress into blastocysts, whereas the blastocyst rate of the wild type could reach  $91.1 \pm 4.1\%$  (Fig. 2B). Most mutant embryos were arrested at different stages before progressing into blastocysts (Fig. 2A,B). *In vivo*, even though a few mutant embryos could implant and develop in the uterus (Fig. 2C), the average number of embryos at E10.5 (Fig. 2D and Table S2) was significantly lower, and ~80% successfully mated mutant female mice even did not have implanted embryos.

### Depletion of PPP4C impairs genomic integrity in oocytes and fertilized eggs

As PPP4C is involved in DNA damage repair, we hypothesized that the genomic integrity of normal-looking oocytes and zygotes of *Ppp4c* mutant mice had been impaired. Single-cell gel electrophoresis (comet assay) was used to quantify the extent of unrepaired DNA damage in GV and metaphase II (MII) oocytes. As expected, GV and MII oocytes of Zko female mice showed large amounts of DNA damage; the amount of comet tail DNA increased 2.6- and 4.6-fold, respectively, when quantified using CASP software (Fig. 3A-F). Although a few lesions existed in GV oocytes of wild type, as indicated by elongated comet tail (Fig. 3A,B), the lesions were not found in MII oocytes (Fig. 3D,E). So we speculated that there might be DNA repair during oocyte maturation. We assessed  $\gamma$ H2AX, a marker of DNA damage (McManus and Hendzel, 2005), during oocytes maturation using chromatin spread preparations. Unfortunately, as shown in Fig. S3A,  $\gamma$ H2AX is not a good marker for DNA damage in

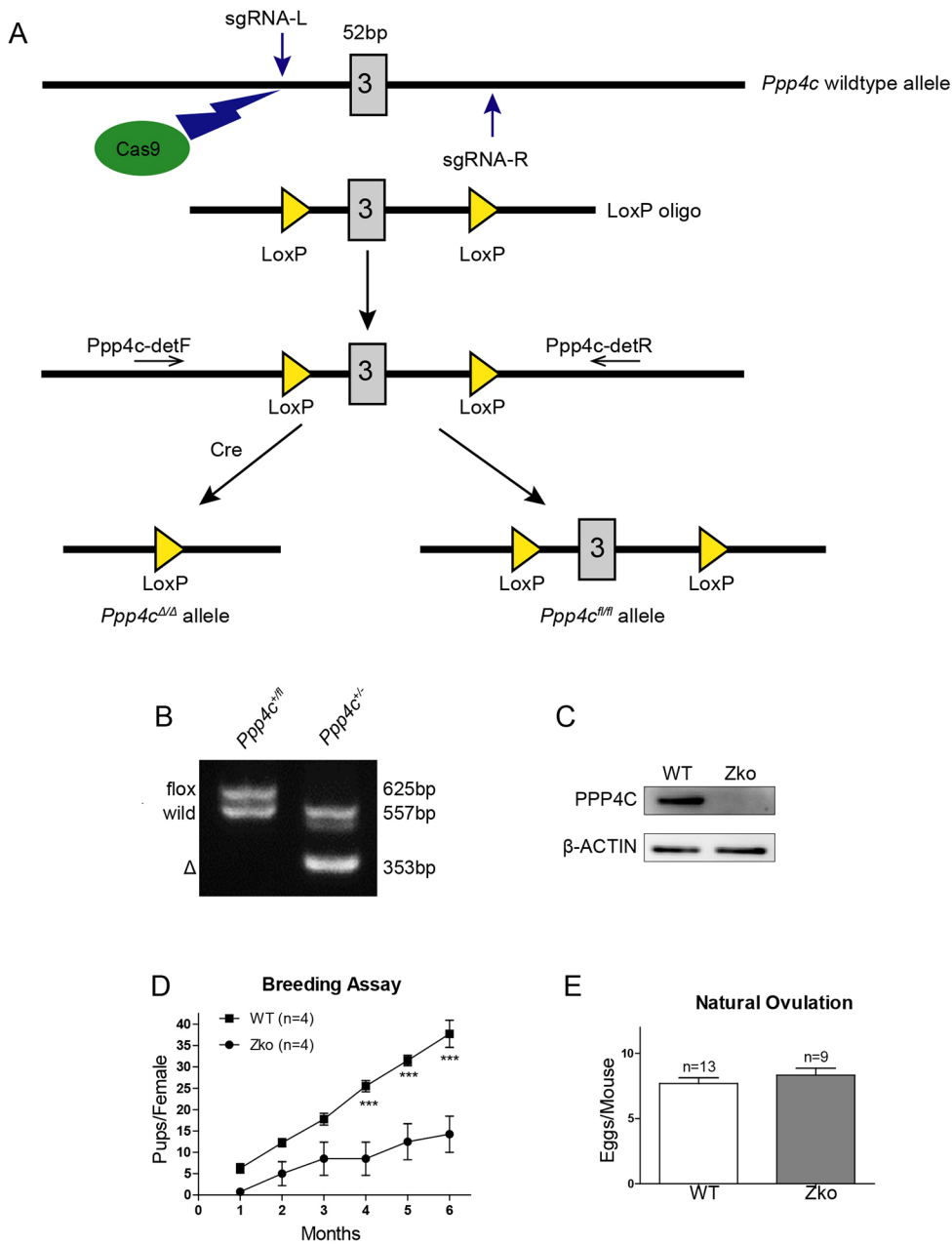


**Fig. 1. Generation and fertility of *Ppp4c* conditional knockout mouse line.**

(A) Schematic of strategy for generating a *Ppp4c* conditional knockout mouse. (B) PCR genotyping of floxed allele, wild-type allele and  $\Delta$  allele, corresponding to 625 bp, 557 bp and 353 bp, respectively. (C) Western blotting performed with wild-type and Zko oocytes with antibodies against PPP4C showed highly reduced expression of PPP4C in Zko oocytes. (D) Reduced fertility of Zko female mice. Continuous breeding showed the cumulative number of pups per female mouse over 6 months. Four mice of each genotype were used. (E) Natural ovulation of Zko female mice. Fertilized eggs were collected and counted from females with vaginal plugs after mating. Data are mean  $\pm$  s.e.m. \*\*\* $P < 0.001$ . The total numbers of analyzed mice are indicated (n).

metaphase. To determine whether PPP4C was involved in DNA repair in mouse zygotes,  $\gamma$ H2AX was assessed in zygotes of relevant pronuclear (PN) stages by staining. Mouse zygotes were obtained at 22 h (PN2), 24 h (PN3), 28 h (PN4) and 30 h (PN5) post-hCG and stained with anti- $\gamma$ H2AX antibody, as previously described (Xu et al., 2015). In wild-type zygotes,  $\gamma$ H2AX foci initially appeared at the PN2 stage, and dramatically increased at PN3 and PN4 stages, and almost disappeared at the late PN5 stage (Fig. 3G and Fig. S3B, left panel). However, compared with the wild type at PN2 and late PN5 stages,  $\gamma$ H2AX foci persisted in PPP4C-deficient zygotes (Fig. 3G-I, Fig. S3B). This also indicated that the DNA damage in embryos may come from two sources: DNA damage remaining in oocytes and DNA replication in zygotes.

#### Formation of micronuclei in PPP4C-deficient 2-cell embryos

As most of PPP4C-deficient embryos were arrested at different stages and about half of them (43.14% $\pm$ 0.08 at E2.5) were arrested at the

two-cell stage (Fig. 2B), we then investigated the role of PPP4C in DNA repair at the two-cell stage. A primary function of the cell cycle is replication of the genome and it is divided into four phases: G1, S, G2 and M. To determine the cell-cycle dynamics of two-cell embryos, we used BrdU labeling. As shown in Fig. 4A, cell entry into S phase occurred almost immediately after one-cell division, and DNA replication was completed after about 9 h. PPP4C deficiency did not affect the replication process. To determine whether PPP4C was involved in DNA repair in two-cell embryos,  $\gamma$ H2AX was assessed by staining. We analyzed the  $\gamma$ H2AX foci in the G2 phase of two-cell embryos, in which endogenous DNA lesions have been repaired or are being repaired (Lindahl and Barnes, 2000; Derijck et al., 2008) and  $\gamma$ H2AX has been dephosphorylated (Xu et al., 2015). However, the observed accumulation of  $\gamma$ H2AX (Fig. 4B,C) demonstrated that DNA lesions could not be repaired in the G2 phase of two-cell PPP4C-deficient embryos. We further observed that numerous abnormal micronuclei existed in the PPP4C-deficient

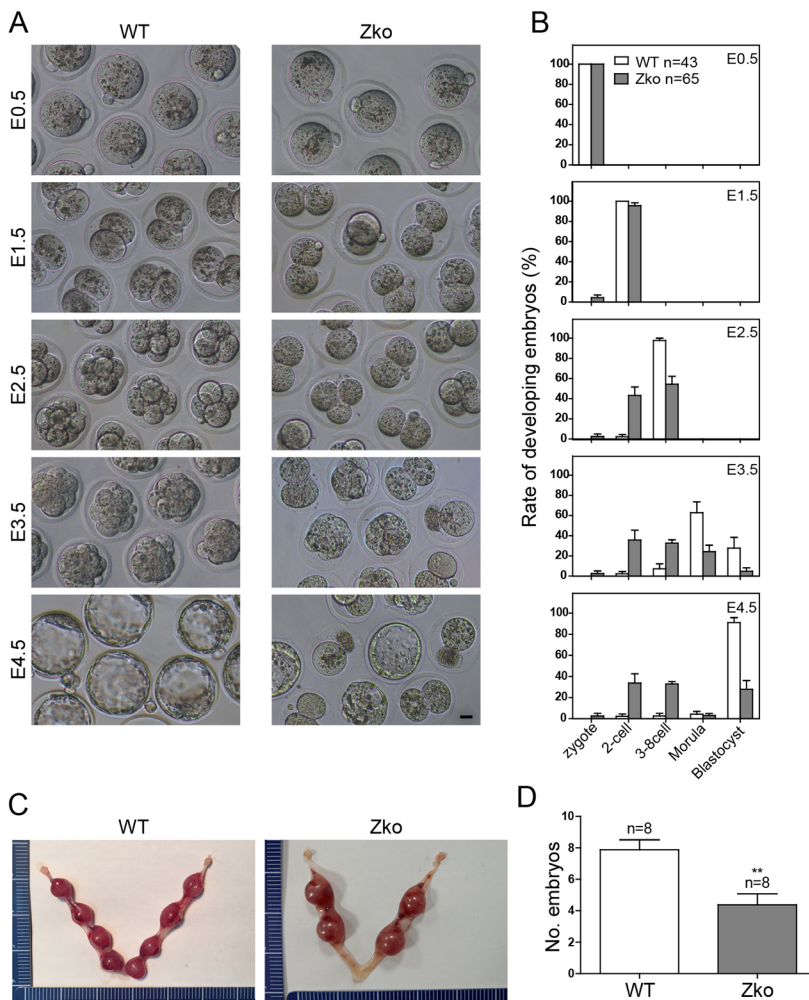


**Fig. 2. Maternal depletion of PPP4C leads to embryo development arrest.** (A,B) Wild-type and Zko females were super-ovulated and mated with normal fertile males. Embryos were collected at E0.5 and cultured in KSOM medium *in vitro*. The developmental stages of embryos were judged according to blastomere numbers. Rates of developing embryos at different stages derived from at least five females are shown. Data are mean±s.e.m. from three independent experiments. Scale bars: 20 µm. (C) Representative images of embryos at E10.5 from wild-type and Zko females are shown. (D) The number of embryos in the uterus at E10.5. Data are mean ±s.e.m. \*\* $P < 0.01$ . The total numbers of analyzed mice are indicated (*n*).

two-cell embryos (Fig. 4D,E), which might be caused by severe genomic rearrangements and chromosome fragmentation (Zhang et al., 2015).

### PPP4C deficiency induces sustaining CDK1 activity and influences RAD51 recruitment

According to the classic theory, NHEJ is used primarily in the G1 phase of the cell cycle and HR is used primarily in the S and G2 phase (Symington and Gautier, 2011). In addition, according to our results (Fig. 4A) and to a previous report, mouse early cleavages are characterized by a short G1 phase (Artus and Cohen-Tannoudji, 2008). We speculated that the PPP4C deficiency might cause HR defects. To confirm the hypothesis, we analyzed the two critical steps of HR – DNA end resection and ssDNA invasion – which were marked with RPA2 and RAD51, respectively (Ciccia and Elledge, 2010). As shown in Fig. 5A–C, depletion of PPP4C induced RPA2 (a DNA end resection marker) foci accumulation in the nuclei of the G2 phase of two-cell embryos, and this was not replaced by RAD51 (a ssDNA invasion marker) when DNA exhibited etoposide (Etop)-induced lesions. This demonstrated that DNA end resection had taken place and ssDNA invasion was prevented by PPP4C deficiency, so HR could not take place. To assess whether DNA synthesis was influenced in PPP4C-deficient embryos, G2-phase two-cell embryos were stained using anti-FANCD2 antibody, a marker of DNA synthesis. As shown in Fig. S4A, DNA synthesis could not be completed in PPP4C-deficient G2-phase two-cell embryos.

On the one hand, CHK1 directly regulates RAD51 by phosphorylating its Thr309 (Sørensen et al., 2005); on the other hand, assembly of RAD51 filaments on RPA2-coated ssDNA is mediated by BRCA2 (West, 2003), and the CDK-dependent phosphorylation of BRCA2 C terminus is very important for the interaction between RAD51 and BRCA2 (Esashi et al., 2005). So we assessed relevant phosphorylated protein expression by western immunoblotting to investigate which regulatory protein was responsible for the defective RAD51 assembly in the G2 phase. In PPP4C-deficient two-cell embryos, CHK1 could be duly activated in response to DNA damage (Fig. 5D,E). However, the activity of CDK1 was not inhibited (Fig. 5D). No matter whether the two-cell embryos were treated with Etop or not, CDK1 still maintained a higher activity and the S3291 site of BRCA2 was phosphorylated in PPP4C-deficient G2-phase two-cell embryos (Fig. 5F and Fig. S4B), which blocked the interaction between BRCA2 and RAD51.

Paradoxically, it has been reported that CHK1 could phosphorylate the protein phosphatase CDC25 to inhibit the activity of CDK1 (Sanchez et al., 1997), i.e. there are other signaling pathways participating in regulating CDK1 in early embryos. We also assessed the activation status of CHK2, another DNA damage checkpoint kinase that also regulates the activity of CDK1 through CDC25 (Karlsson-Rosenthal and Millar, 2006). Normally, when DNA is damaged in cells, the two checkpoint kinases (CHK1 and CHK2) are activated, triggering cell cycle arrest to allow cells to have enough time for repair. So factors (e.g. CDC25

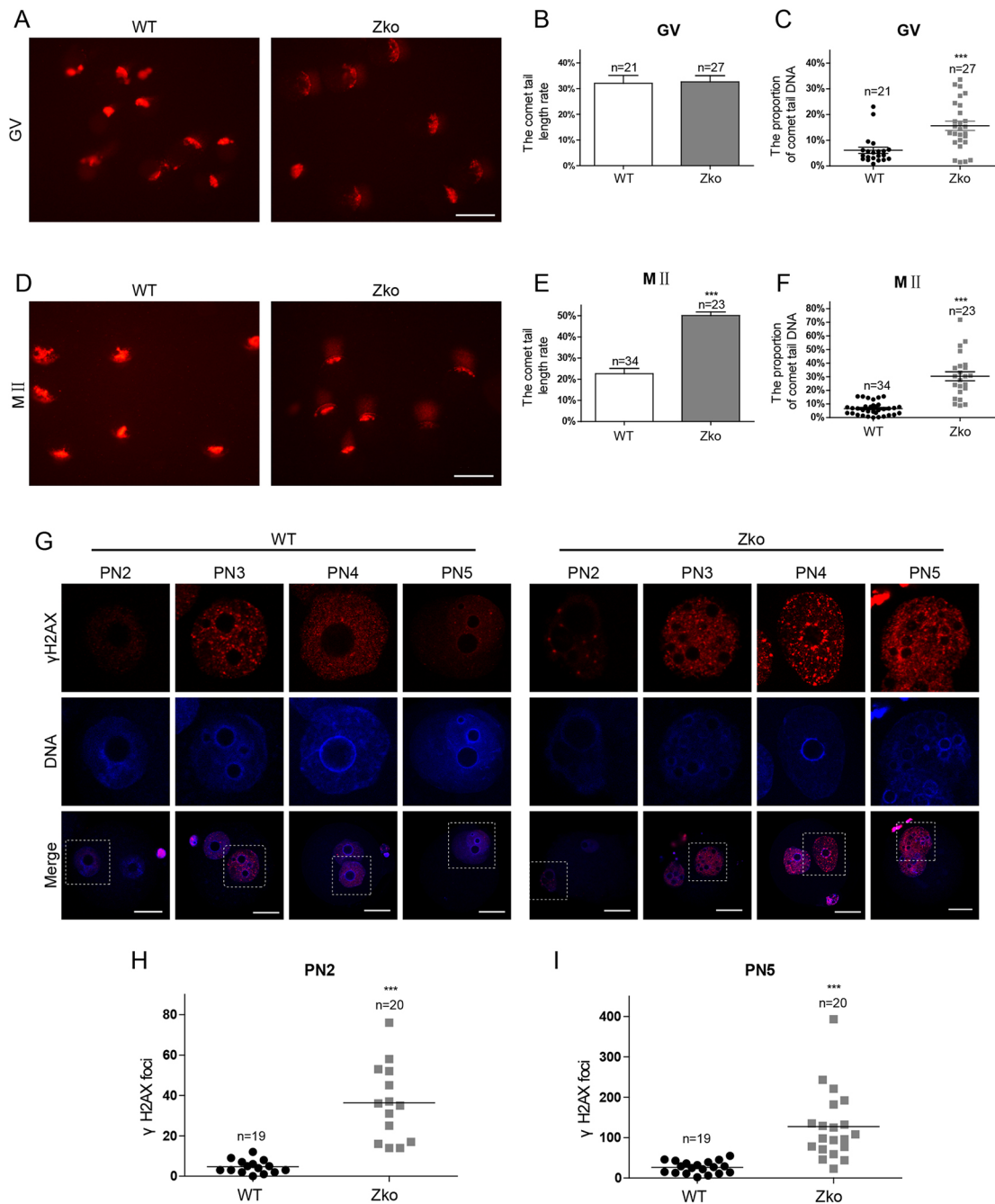


**Fig. 3. Depletion of PPP4C impairs genomic integrity of oocytes and fertilized eggs.** (A-C) The GV oocytes of representative images are shown. The comet tail length and DNA proportion were quantified using CASP software. Wild-type and Zko females were analyzed by single-cell gel electrophoresis (comet assay). Representative images are shown. The comet tail length and DNA proportion were quantified using CASP software (length rate = tail length/total length). (D-F) MII oocytes of wild-type and Zko females were analyzed by single-cell gel electrophoresis (comet assay). (G) Zygotes of wild-type and Zko females were obtained at 22, 24, 28 and 30 h post-hCG and stained with anti- $\gamma$ H2AX antibody. (H,I) Quantification of  $\gamma$ H2AX foci in both pronuclei of individual zygotes obtained at PN2 or PN5 stage, respectively. Data are mean  $\pm$  s.e.m. from three independent experiments. The total numbers of analyzed zygotes are indicated (*n*). \*\*\**P* < 0.001. Scale bars: 100  $\mu$ m in A,D; 20  $\mu$ m in G.

and CDK) governing cell cycle progression are required to inactivate temporarily. However, as shown in Fig. 5G and Fig. S6A, PPP4C deficiency blocked the activation of CHK2 to respond to DNA damage, and enhanced the activity of CDC25B (Fig. 5H, Fig. S6B) when DNA in G2-phase two-cell embryos exhibited induced lesions following treatment with 10 Gy X-ray. These results suggest that sustaining CDK1 activity might be caused by the defective response of CHK2 to DNA damage.

#### DNA damage in PPP4C-deficient embryos could be rescued by inhibition of PLK1

As reported previously (van Vugt et al., 2010), PLK1 could regulate the activation status of CHK2 by binding 53BP1 during the G2/M phase transition. Therefore, we hypothesized that sustaining PLK1 activity might induce CHK2 inactivation in PPP4C-deficient embryos and performed a rescue experiment to confirm this point. As shown in Fig. 6A and Fig. S6C, the failure of the CHK2

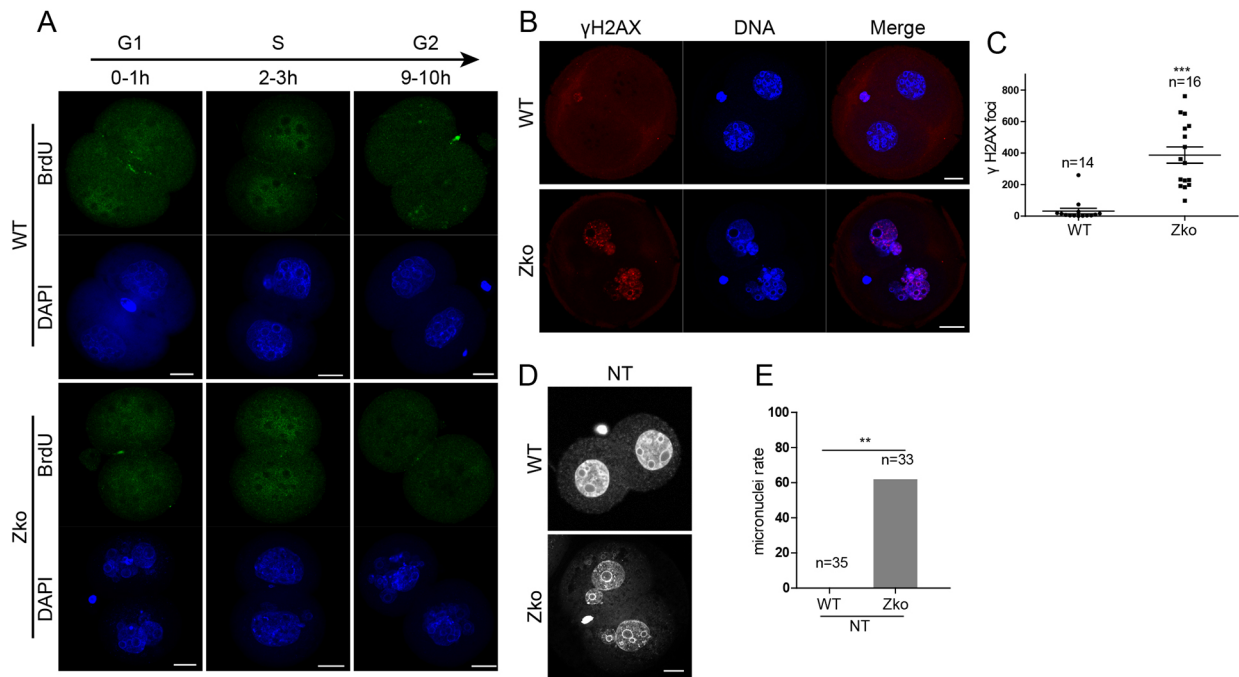


**Fig. 4. PPP4C is required for DNA repair in mouse embryos.** (A) Dynamics of BrdU staining during the two-cell phase of wild-type and Zko groups. Embryos were pre-treated with BrdU for 1 h before staining. (B) Representative images of  $\gamma$ H2AX foci in G2 phase of two-cell embryos in wild-type and Zko groups. (C) Quantification of  $\gamma$ H2AX foci in B was analyzed with Imaris software. (D) Representative images of micronuclei in G2 phase of two-cell embryos in wild-type and Zko groups. (E) Quantification of cells displaying micronuclei in D. Data are mean $\pm$ s.e.m. from three independent experiments. \*\* $P$ <0.01 and \*\*\* $P$ <0.001. The total numbers of analyzed embryos are indicated ( $n$ ). Scale bars: 20  $\mu$ m.

checkpoint in PPP4C-deficient two-cell G2 embryos was rescued by inhibition of PLK1 for 3 h. Moreover, the failure of RAD51 recruitment in PPP4C-deficient G2 phase two-cell embryos was also rescued by inhibition of PLK1 or CDK1 (Fig. 6B-D), when embryos were treated with Etop and a PLK1 inhibitor, BI2536, or a CDK1 inhibitor, Ro3306, for 3 h before staining. Definitively,  $\gamma$ H2AX and RPA2 foci could both be erased in PPP4C-deficient embryos by inhibition of PLK1 or CDK1 (Fig. 6E-G). To demonstrate that the failure of RAD51 recruitment is due to the inactivation of CHK2 in PPP4C-deficient embryos, we performed an inhibition experiment. As shown in Fig. 6H, inhibition of CHK2 with BML-277 prevented RAD51 recruitment when two-cell embryos were treated with Etop for 3 h. In addition, inhibition of CHK2 with BML-277 also prevented RAD51 rescue in PPP4C-deficient two-cell embryos when co-treated with BI2536 and Etop for 3 h (Fig. 6I). However, RPA2 appeared as aberrant spreading in the nuclei rather than as a typical homogenous sphere when treated with BI2536, indicating that the arrangement of RPA2 was disrupted and its recruitment might involve PLK1 activity.

#### DNA end resection requires PLK1 activity

Post-resection CDK1 inhibition is important for the second phase of HR, but CDK1 activity is also required for DNA end resection – one of the initial events in HR (Huertas et al., 2008; Huertas and Jackson, 2009; Ferretti et al., 2013; Wang et al., 2013; Buisson et al., 2017). There has been little direct evidence showing that PLK1 activity is also required for DNA end resection. To address this, we first analyzed the  $\gamma$ H2AX and RPA2 foci in S-phase two-cell embryos between the control and PPP4C-deficient groups. As shown in Fig. 7A,B, PPP4C deficiency resulted in more serious DNA damage and resection in S-phase two-cell embryos. However, inhibition of PLK1 starting at the G1 phase affected RPA2

recruitment to the DNA damage site and RAD51 could not be loaded (Fig. 7C), which demonstrated that PLK1 activity was required for DNA end resection. More importantly, inhibition of PLK1 after the G1 phase affected the DNA damage response, so that two-cell embryos could not form  $\gamma$ H2AX foci when treated with Etop (Fig. S4C).

#### PPP4C interacts with PLK1 in the context of DNA damage, and knocking out PPP4C enhances PLK1 phosphorylation

It has been reported that S137 and T210 are two major phosphorylation sites in activated PLK1 (Jang et al., 2002; Lowery et al., 2005). We speculated that PLK1 may be a substrate of PPP4C, and PPP4C depletion increases the level of phosphorylation of PLK1. To test this hypothesis, MYC-PPP4C and HA-PLK1 were expressed in 293T cells by transfecting indicated plasmids for co-immunoprecipitation (co-IP) experiments. As expected, regardless of whether anti-MYC antibody or anti-HA antibody was used for co-IP, we observed clear co-IP between PPP4C and PLK1 (Fig. 8A). Using the NICIF assay, a protein phosphorylation prediction method related to the isoelectric point (pI) of a protein, we determined that the PLK1 peaks reflected post-translational modification (PTM) of PLK1 changes in the G2 phase of two-cell embryos between wild-type and PPP4C-deficient mice (Fig. S5). Disappearance of the pI 8.8 peak indicated that high level phosphorylation of PLK1 might exist in PPP4C-deficient two-cell embryos. To test whether the activity of PLK1 was affected by PPP4C deficiency, we assessed the phosphorylation status of S137 and T210 sites in PLK1 by western immunoblotting (Fig. 8B, Fig. S6D). S137 phosphorylation was detectable at a higher level when wild-type two-cell embryos were untreated and decreased when treated with Etop for 3 h. However, in the absence of PPP4C, the S137 site remained phosphorylated at an elevated level regardless of whether two-cell embryos were treated

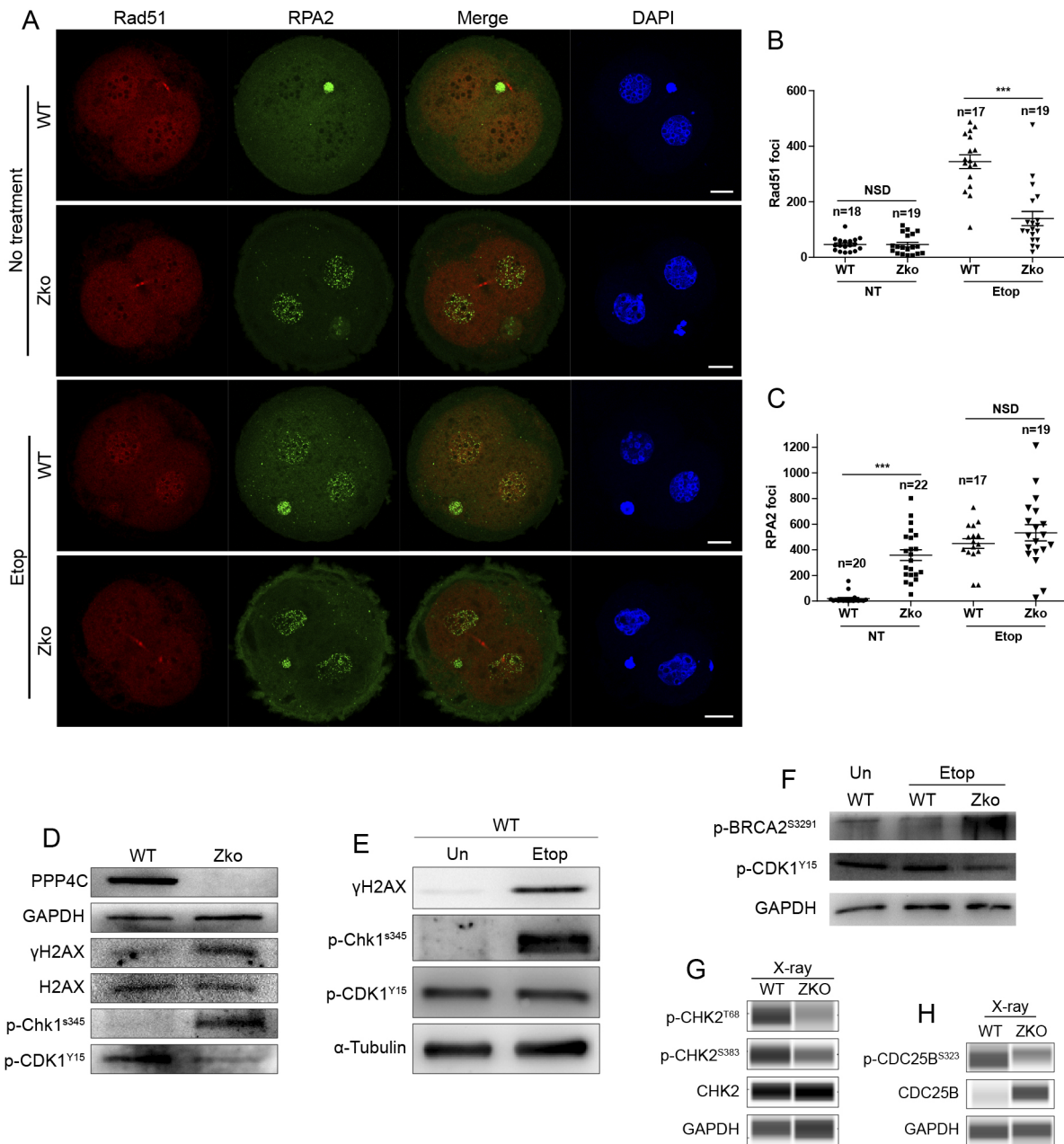


**Fig. 5. PPP4C deficiency induces sustained CDK1 activity and influences RAD51 recruitment.** (A) Representative images of RAD51 and RPA2 foci in G2 phase of two-cell embryos in wild-type and Zko groups. Embryos were treated with or without Etop for 3 h before staining. Scale bars: 20  $\mu$ m. Quantification of RAD51 (B) and RPA2 (C) foci in A was analyzed with Imaris software. Data are mean $\pm$ s.e.m. from three independent experiments. \*\*\* $P$ <0.001. The total numbers of analyzed embryos are indicated ( $n$ ). (D) PPP4C deficiency induced DNA damage and CHK1 activated, but did not inhibit CDK1 activity. Levels of the indicated proteins in G2 phase of two-cell embryos were analyzed by western blot. (E) DNA damage results in CHK1 activation and CDK1 deactivation in wild-type embryos. Levels of the indicated proteins in G2 phase of two-cell embryos in the wild type were analyzed by western blot. Embryos were treated with or without Etop for 3 h before harvest. (F) Activated CDK1 in PPP4C-deficient two-cell embryos induced BRCA2 S3291 hyper-phosphorylation. Levels of the indicated proteins in the G2 phase of two-cell embryos were analyzed by western blot. (G) PPP4C deficiency affected CHK2 activity. Levels of the indicated proteins in the G2 phase of the two-cell embryos were analyzed by automated western immunoblotting. Embryos were treated with a 10 Gy X-ray and harvested 1 h later. (H) PPP4C deficiency induced sustained CDC25 activity in the G2 phase of two-cell embryos after 1 h irradiation with 10 Gy. Levels of the indicated proteins were analyzed by automated western immunoblotting.

with Etop, and BI2536 could decrease its phosphorylation level. Puzzlingly, T210 phosphorylation remained at lower levels when wild-type two-cell embryos were untreated, and increased when treated with Etop for 3 h. PPP4C deficiency prevented the tendency of T210 to be phosphorylated, but not significantly. Together, these results clearly show that, in response to DNA damage, PPP4C might directly dephosphorylate PLK1 at the S137 site. But we do not know

the relationship between the two sites of PLK1 when DNA displays damage.

#### Phosphorylation of PLK1 at S137 and T210 influences RPA2 and RAD51 recruitment

To understand how the phosphorylation status of S137 and T210 affects HR in two-cell embryos, we analyzed cells expressing a set

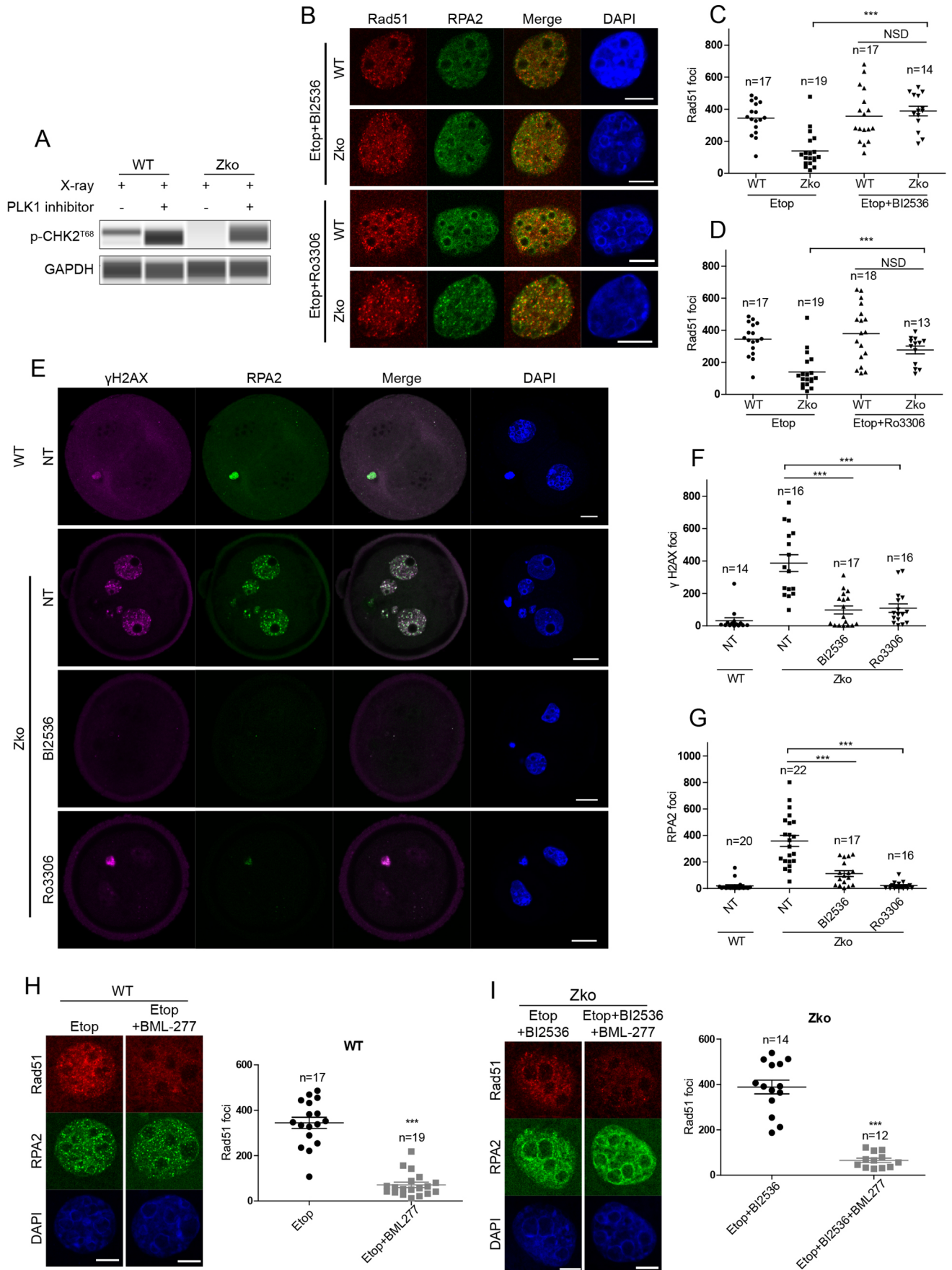


Fig. 6. See next page for legend.



**Fig. 6. DNA damage in PPP4C-deficient embryos could be rescued by inhibition of PLK1.** (A) The failure of the CHK2 checkpoint in PPP4C-deficient G2 phase two-cell embryos was rescued by inhibition of PLK1. Embryos were treated with or without a PLK1 inhibitor, BI2536, for 2 h before irradiation with a 10 Gy X-ray and maintained for 1 h before harvest. Levels of the indicated proteins were analyzed by automated western immunoblotting. (B) The failure of RAD51 recruitment in PPP4C-deficient G2 phase two-cell embryos is rescued by inhibition of PLK1 or CDK1. Embryos were treated with Etop and BI2536 or Ro3306 (CDK1 inhibitor) for 3 h before staining. (C,D) Quantification of RAD51 foci in B was analyzed with Imaris software. (E)  $\gamma$ H2AX and RPA2 foci were erased by inhibition of PLK1 or CDK1. Embryos were treated with BI2536 or Ro3306 for 3 h before staining. (F,G) Quantification of  $\gamma$ H2AX (F) and RPA2 (G) foci in E was analyzed with Imaris software. (H) Inhibition of CHK2 with BML-277 prevents RAD51 recruitment when two-cell embryos were treated with or without Etop. (I) Inhibition of CHK2 with BML-277 prevents RAD51 rescue in PPP4C-deficient two-cell embryos. Scale bars: 10  $\mu$ m in B,H,I; 20  $\mu$ m in E. Data are mean  $\pm$  s.e.m. from three independent experiments. \*\*\* $P$ <0.001. The total numbers of analyzed embryos are indicated ( $n$ ).

of PLK1 variants, including wild type (PLK1<sup>WT</sup>), a phospho-null mutant in S137 site (PLK1<sup>S137A</sup>), a phosphomimetic mutant in the S137 site (PLK1<sup>S137D</sup>), and a phosphomimetic mutant in both S137 and T210 sites (PLK1<sup>STDD</sup>). The substitution of either T210 or S137 with Asp elevates the kinase activity of PLK1. However, the substitution of S137 with Ala decreases the kinase activity (Jang et al., 2002). Wild-type zygotes were collected 24 h post-hCG and injected with the sets of PLK1 variants. These zygotes cleaved into two-cell embryos without obvious developmental delay (data not shown). However, the two-cell embryos expressing PLK1<sup>S137D</sup> and PLK1<sup>STDD</sup> showed increased RPA2 and  $\gamma$ H2AX foci, and few RAD51 foci compared with those expressing PLK1<sup>WT</sup> in G2 phase (Fig. 8C-F). This suggests that sustaining activation of PLK1 leads to failure of RPA2-coated ssDNA replacement by RAD51. In addition, expressing PLK1<sup>S137A</sup> abolished the recruitment of RPA2 to DNA repair foci in Etop-treated G2-phase two-cell embryos (Fig. 8D), which resembled the phenotype of inhibition of PLK1 since the G1 phase (Fig. 7C).

Together, these data demonstrate that the process of HR requires not only the activation but also the inactivation of PLK1, during which PPP4C is responsible for the transition. PLK1 activation is needed to maintain CDK1-dependent resection when cells are facing DNA damage and replication stress. However, sustaining CDK1 activation blocks RAD51 recombination activity by phosphorylating the S3291 site of BRCA2. As the HR continues, PPP4C suppresses the activity of PLK1 by dephosphorylating the S137 site. DNA damage in the checkpoint protein results in inhibition of CDK1 activity, followed by activation of BRCA2 and RAD51 focus formation.

## DISCUSSION

PPP4 plays important roles in the DNA damage response, as previously reported (Chowdhury et al., 2008; Nakada et al., 2008; Lee et al., 2010; Liu et al., 2012; Lee et al., 2014). PPP4 has been shown to contribute to DNA damage repair by dephosphorylating  $\gamma$ -H2AX, RPA2, 53BP1 and KAP-1, which regulate the essential steps in DNA damage repair. As two major pathways for DSB repair, NHEJ is used primarily in the G1 phase of the cell cycle, while HR is used primarily in the S and G2 phases (Symington and Gautier, 2011). We investigated the role of PPP4C in HR of early mammalian embryos by minimizing its impact on NHEJ, because mouse early cleavages are characterized by a short G1 phase (Artus and Cohen-Tannoudji, 2008).

In this study, we show that: (1) PPP4C, as protein phosphatase 4 catalytic subunit, is dispensable for oocyte growth and meiotic

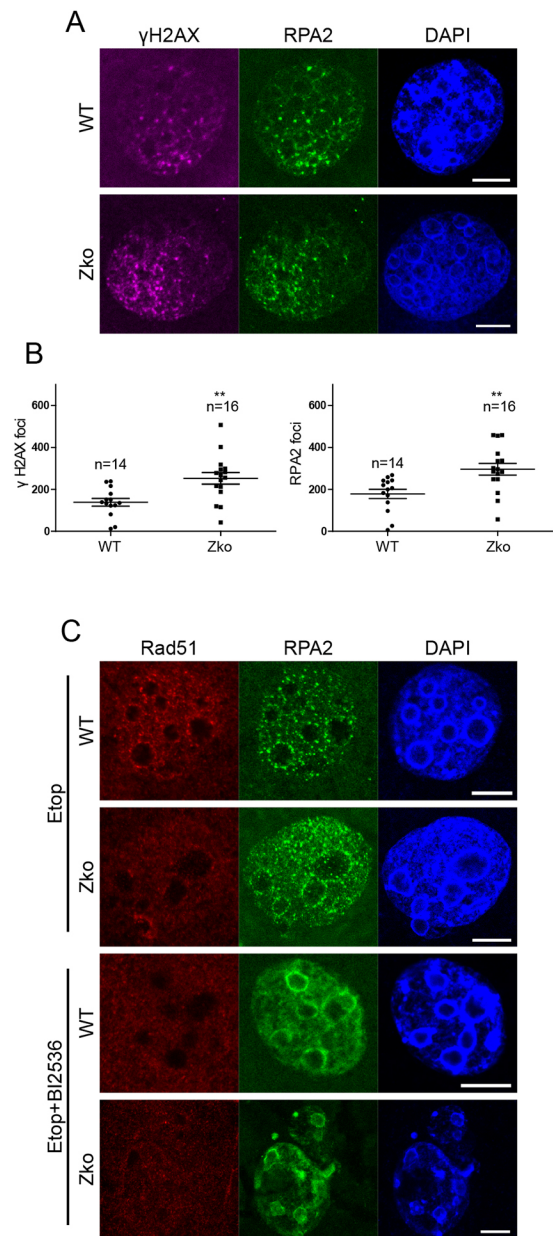


**Fig. 7. DNA end resection requires PLK1 activity.** (A,B) PPP4C deficiency results in more serious DNA damage and resection in S phase of two-cell embryos. (A) Representative images of  $\gamma$ H2AX and RPA2 foci. Embryos were fixed after 3 h when embryos entered the two-cell phase. (B) Quantification of  $\gamma$ H2AX and RPA2 foci was analyzed with Imaris software. Data are mean  $\pm$  s.e.m. from three independent experiments. \*\* $P$ <0.01. The total numbers of analyzed embryos are indicated ( $n$ ). (C) Inhibition of PLK1 after G1 phase affected RPA2 recruitment to the DNA damage site and RAD51 could not be loaded. Embryos were treated with or without BI2536 after G1 phase, and DNA damage was induced with Etop for 3 h in G2 phase before staining. Scale bars: 10  $\mu$ m.

maturation, but the genome integrity of MII oocytes is damaged due to the absence of PPP4C; (2) PPP4C dysfunction induces HR failure along with embryo development arrest at different cleavage stages; (3) PPP4C mediates de-phosphorylation of PLK1 at the S137 site and regulates its inactivation in HR; and (4) the activity of PLK1 is dynamically changed during HR, during which high PLK1 activity promotes DNA end resection and low PLK1 activity guarantees RAD51 recruitment by regulating the CHK2-CDC25-CDK1 pathway.

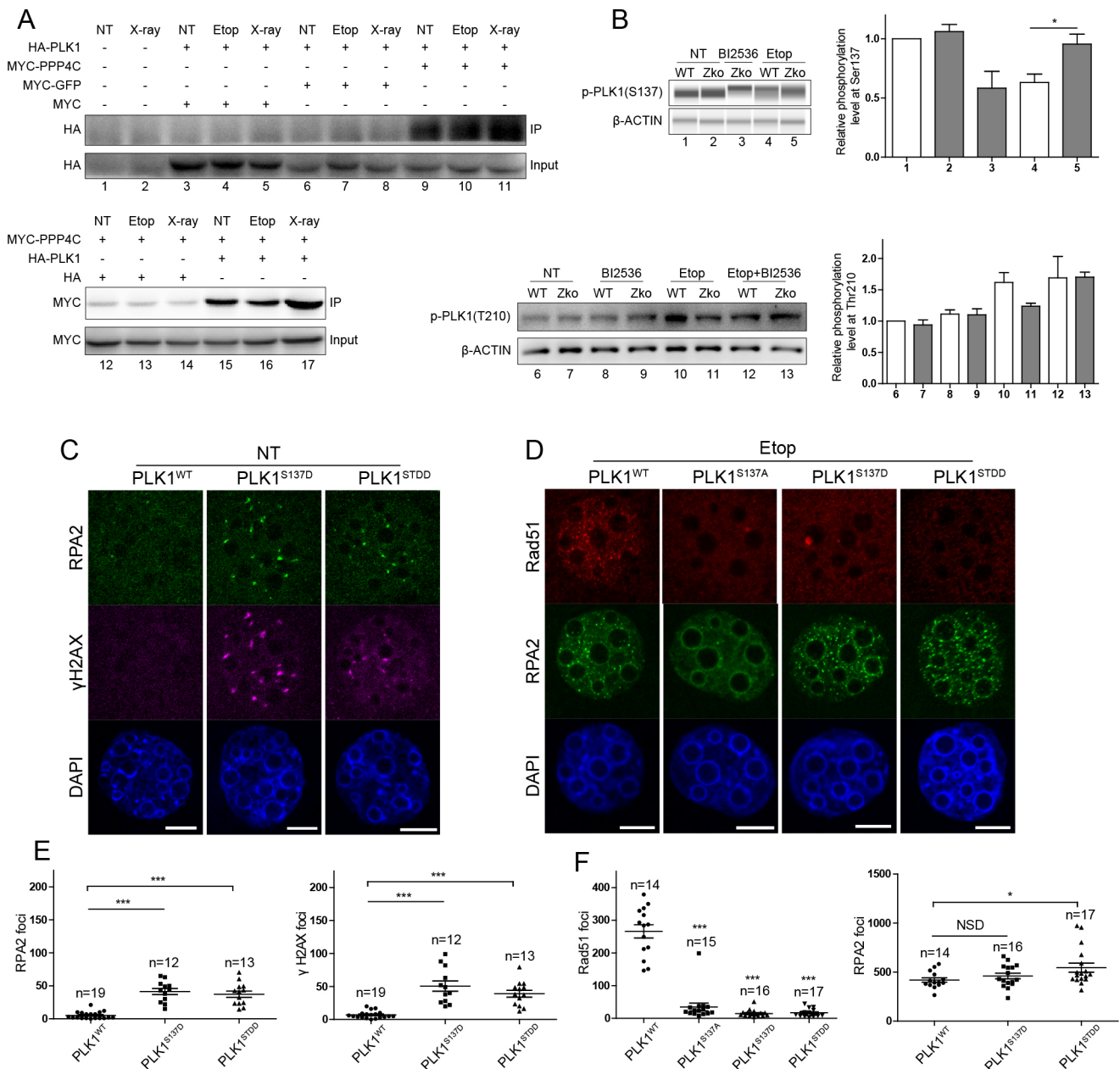


**Fig. 8. PPP4C interacts with PLK1 and dephosphorylates PLK1 when cells exhibit DNA damage.** (A) (Top) Co-immunoprecipitation from 293T cells where HA-tagged PLK1 was stably expressed. Anti-MYC antibody was used for co-immunoprecipitation in untreated (NT), Etop- or X-ray-treated cells, and the western blot was probed with anti-HA antibody. The negative controls were wild-type 293T cells or 293T cells transfected with expression vectors for MYC and HA-PLK1, or for MYC-GFP and HA-PLK1. (Bottom) Co-immunoprecipitation of 293T cells where MYC-tagged PPP4C was stably expressed. Anti-HA antibody was used for co-immunoprecipitation from untreated (NT), Etop- or X-ray-treated cells and the western blot probed with anti-MYC antibody. The negative controls were 293T cells transfected with expression vectors for HA and MYC-PPP4C. (B) PPP4C deficiency induced sustained phosphorylation of PLK1 at the S137 site and reduced the tendency of T210 to be phosphorylated, but not significantly. Levels of the indicated proteins in the G2 phase of two-cell embryos were analyzed by western blot. (C,E) Formation of RAD51, RPA2 and  $\gamma$ H2AX foci in no-treatment wild-type two-cell embryos expressing PLK1 variants. (D,F) Formation of RAD51 and RPA2 foci after Etop treatment of wild type two-cell embryos expressing PLK1 variants. WT, wild type PLK1; S137D, S137 mutation to aspartate; S137A, S137 mutation to alanine; STDD, S137 and T210 both mutated to aspartate. Data are mean $\pm$ s.e.m. from three independent experiments. \* $P$ <0.05, \*\*\* $P$ <0.001. The total numbers of analyzed embryos are indicated ( $n$ ). Scale bars: 10  $\mu$ m.

Actually, it is not difficult to understand that the activity of PLK1 is dynamically changed during DDR. Mounting studies have provided evidence that PLK1 is crucial for mitotic entry following recovery from DNA damage (van Vugt et al., 2004; Yoo et al., 2004; Syljuåsen et al., 2006; Macürek et al., 2008; Seki et al., 2008). DNA damage-mediated cell-cycle arrest allows time to repair DNA lesions, and PLK1, as a cell cycle-promoting factor, is important for inactivation

during DDR. Indeed, when cells were treated with DNA damaging agents, PLK1 is inhibited and dephosphorylated (Smits et al., 2000; Yuan et al., 2004; Jang et al., 2007). But the most recent studies have established the role for PLK1 immediately after DNA damage: PLK1-mediated RAD51 phosphorylation facilitates its recruitment to damage sites (Yata et al., 2012; Peng et al., 2021). Additionally, PLK1 could enhance BTR-mediated dissolution of recombination

intermediates and curtail genomic instability at the G2/M transition. In meiotic cells, PLK1 depletion increased crossover recombination and aberrant SC processes. So it is conceivable that the activity of PLK1 is dynamically changed and de-phosphorylation of PLK1 by protein phosphatase coordinates DNA repair and cell-cycle progression.

During the DNA repair process, PLK1, CDC25 and CDK1 form a feedback loop and positively regulate the activity of one another (Murray, 2004; Seki et al., 2008). Several reports have indicated that the DSB repair pathway choice between NHEJ and HR is dependent on the regulation of CDK1 (Jazayeri et al., 2006; Chapman et al., 2012; Escribano-Díaz et al., 2013); e.g. CDK1 triggers DSB resection by both counteracting the inhibitory effect of the NHEJ proteins and stimulating the activity of the DSB resection machinery (Trovesi et al., 2013). In both budding and fission yeast, CDK1-dependent phosphorylation of *Sae2*, which is the homologous gene of CtIP (*Rbbp8*) in mammals, is needed to remove Ku from DSB ends in order to allow the action of EXO1 and Sgs1 (Huertas et al., 2008; Mimitou and Symington, 2010; Trovesi et al., 2013). In addition, CDK1 can promote extensive resection by counteracting the inhibitory activity of Rad9 (Mimitou and Symington, 2010; Trovesi et al., 2013), which is the homologous gene of 53BP1 (*Trp53bp1*) in mammals.

In human cells, DSB end resection also requires the regulation of CDKs (Huertas and Jackson, 2009), but it must be inactivated after DNA end resection, which allows Rad51 and BRCA2 to interact and use the RPA-coated ssDNA to initiate HR (Esashi et al., 2005; Jazayeri et al., 2006; Buisson et al., 2017). Remi et al. provided a model in which HR is a biphasic process requiring both high-CDK and low-CDK periods (Buisson et al., 2017). In brief, when the genome is facing DNA damage and replication stress in the S/G2 phase, CDK1 is transiently activated to promote Ku release from

DSB and CtIP-mediated DNA end resection. With the ssDNA generation and RPA recruitment, ATR is activated, which suppresses CDK1 through Chk1-mediated degradation or inhibition of CDC25 phosphatases, and phosphorylates HR substrates (Buisson et al., 2017). In addition to CHK1, the upstream factors of CDC25 also involve ATM-CHK2, p38-MK2 and PIM1-c-Tak1 (Karlsson-Rosenthal and Millar, 2006). Furthermore, there are three CDC25 isoforms in vertebrates. The regulatory mechanism between DNA damage checkpoint and the cell cycle therefore remains to be further elucidated.

As shown in Fig. 9A,B, CDK1 activity is dynamic during development. In the transition from S to G2 phase, DNA end resection initiated by ATM-MRN occurs in the high-CDK1 period, then checkpoints (CHK1 and CHK2) are triggered by ATR that is recruited to ssDNA by RPA and ATM, respectively. Along with the activation phase of the checkpoint, the cell cycle is arrested by inhibiting CDC25 and CDK1, so cells have enough time to prepare for strand invasion during which RAD51 filaments displace RPA from the 3' ssDNA ends mediated by BRCA2. In our study, we found that one of the two very important checkpoint kinases, CHK2, could not be activated when DNA displays DSBs in PPP4C-deficient embryos. This induced the downstream cell cycle proteins CDC25B and CDK1 to lose their cell cycle inhibitory roles and cells could not carry out DNA repair (Fig. 9C,D). The reason for this was that the upstream regulatory protein of CHK2, PLK1, could not be dephosphorylated at S137 due to PPP4C deficiency. S137 is one of major phosphorylation sites in activated PLK1, so its phosphorylation could enhance the activation of PLK1 and inhibit CHK2 by inactivating its FHA domain (Giunta et al., 2010). Puzzlingly, we do not know why the phosphorylation of another major phosphorylation site, T210 in activated PLK1, is inhibited in

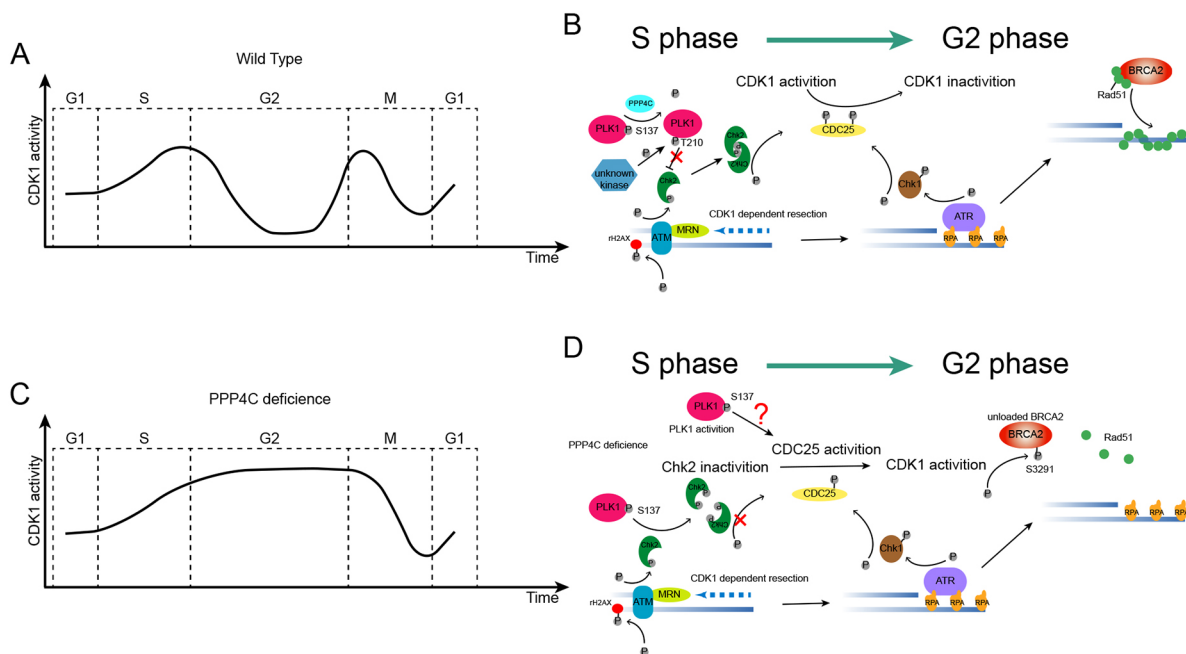


**Fig. 9. A model for the role of PPP4C in HR.** (A,B) In wild-type embryonic cells, the CDK1 activity is dynamic during development. In the transition from S to G2 phase, DNA end resection initiated by ATM-MRN occurs in a high-CDK1 period, then checkpoints (CHK1 and CHK2) are triggered by ATR and are recruited to ssDNA by RPA and ATM, respectively. Along with the activation phase of the checkpoint, the cell cycle is arrested by inhibiting CDC25 and CDK1, so cells have enough time to prepare for strand invasion during which RAD51 filaments displace RPA from the 3' ssDNA ends mediated by BRCA2. (C,D) In PPP4C-deficient cells, the mode of CDK1 activity has been changed and CDK1 keeps sustaining activation in the G2 phase. The reason for this is that the Ser137 site of PLK1 cannot be dephosphorylated due to PPP4C deficiency. The activation of PLK1 is then enhanced, which inhibits CHK2 by inactivating its FHA domain when DNA displays DSBs. Eventually, CDC25B and CDK1 lose inhibition and cells could not carry out DNA repair.

PPP4C-deficient embryos. The relationship of the two sites may need further investigation.

Additionally, the damage in embryos may come from two sources, DNA replication in embryos and the DNA damage remaining in oocytes, because depletion of PPP4C impairs genomic integrity in MII oocytes. These lesions in oocytes may arise from reactive oxygen species during oocyte maturation. PPP4C is predominantly distributed to the nuclei and also expressed in the cytoplasm at the GV stage. During oocyte maturation, PPP4C was mainly distributed in the cytoplasm with no specific localization. This may indicate that PPP4C has a limited role in meiosis. Indeed, the absence of PPP4C in oocytes did not affect oocyte growth and meiotic maturation. As absence of PPP4C contributes to activating CDK1, no matter whether in interphase or M phase, activated CDK1 could phosphorylate RPA2 at S23 and S29 sites, which facilitates exit from a damaged mitosis in the G1 phase (Anantha et al., 2008). Although the interpretation might at first glance be considered counter-intuitive, it was explained that, because interphase RPA2 phosphorylation stimulates DNA repair, RPA modification could similarly promote DNA damage repair in mitotic cells, thereby reducing the DNA damage signal and consequently increasing mitotic exit (Anantha and Borowiec, 2009). We also noticed that some Zko embryos could reach the blastocyst stage or even 10.5 dpc. We speculated this might be due to heterogeneity between oocytes: those with fewer lesions could develop through zygotic genome activation and had limited impairment to genomic integrity. On the other hand, Zp3-Cre is known to be leaky, it is also likely that the extended embryo development could be due to Zp3-Cre leakiness.

Our results not only clarify the important roles of PPP4C in early embryonic development, but also shed light on the regulation of PLK1 by PPP4C during the process of HR. The dephosphorylation of PLK1 by PPP4C is required for efficient activation of CHK2 and inactivation of CDK1 so protein phosphatases might take over the reins of the regulation between cell cycle and DNA repair during the damage response (Campos and Clemente-Blanco, 2020). These findings suggest that more factors should be considered in cancer therapy and that phosphatases may offer new potential targets for cancer treatment.

## MATERIALS AND METHODS

### Mouse maintenance and establishment of the conditional knockout mouse line

All mice care and handling was carried out in compliance with the guidelines of Animal Care and Use Committee of the Institute of Zoology at the Chinese Academy of Sciences. The study was reviewed and approved by the Ethics Committee of the Institute of Zoology, Chinese Academy of Sciences.

To construct a conditional knockout mouse line for targeting the *Ppp4c* allele, exon 3 of *Ppp4c* was flanked by LoxP site using CRISPR/Cas9-Mediated Genome Engineering. In the 648 bp oligo donor sequence, two LoxP (34 bp) sites are inserted 44 bp upstream and 110 bp downstream of exon 3 (52 bp, transcript variant 2), respectively. The homologous arms of the donor were designed as 181 bp and 193 bp. The double strand DNA donor (2 ng/ $\mu$ l), two sgRNAs (50 ng/ $\mu$ l, Table S4) and Cas9 mRNA (60 ng/ $\mu$ l) were then mixed and injected into pronuclei of fertilized eggs maintained on the C57BL/6J background with well-recognized pronuclei in M2 medium (Sigma-Aldrich). The injected zygotes were cultured in KSOM (Millipore) at 37°C under 5% CO<sub>2</sub> in air for approximately 30 min, then 20–25 zygotes were transferred into the uteri of pseudopregnant ICR females at 0.5 dpc. The offspring were genotyped using tail DNA as a PCR templates with two oligo-primers (*Ppp4c*-detF and *Ppp4c*-detR, Table S4; Fig. 2B), and further confirmed by sequencing to obtain *Ppp4c*<sup>+/fl</sup> mice. The conditional knockout mouse line was established by crossing female mice

carrying the conditional allele of *Ppp4c* (*Ppp4c*<sup>fl/fl</sup>) with male transgenic mice (*Ppp4c*<sup>fl/fl</sup>; *Zp3-cre*) expressing the transgene for Cre recombinase specifically in oocytes at primordial stages.

### Breeding assay

In breeding assays, wild-type and Zko genotype female mice at sexual maturity were continually mated to wild C57BL/6J background male mice with known fertility for 6 months. At least four mice of each genotype were used. Unless otherwise stated, all mice used in the following experiments were about 10 weeks old. Cages were checked daily for counting the number of litters and pups. The raw data are provided in Table S2.

### Antibodies and reagents

Antibodies and reagents are shown in Table S3.

### Irradiation and drug treatment

X-ray irradiation was performed on a rad source RS-2000 X-ray irradiator (radiation output at 160 KV, 25 mA 0.3 mm Cu filter; central dose rate 1.13 Gy/min). Zeocin, a Cu-mediated DNA sugar oxidizer (Lin et al., 2014), was added at 10  $\mu$ g/ml in medium when the oocytes or zygotes were cultured. Etoposide (Etop), a topoisomerase inhibitor, was added at 50  $\mu$ g/ml at the indicated time points. BI2536, a PLK1 inhibitor, was added at 200 nM at the indicated time points. Ro3306, a CDK1 inhibitor, was added at 10  $\mu$ M at the indicated time points.

### Immunofluorescence

To analyze chromatin-bound  $\gamma$ H2AX, RPA2 or RAD51, embryos were pre-extracted with ice-cold CSK buffer (He et al., 1990) for 5 min, fixed in 4% paraformaldehyde in PBS for 20 min at room temperature and then blocked in PBS containing 1 mg/ml BSA for 1 h at room temperature. After blocking, the embryos were incubated overnight at 4°C with the antibodies described above at appropriate dilutions. Subsequently, the embryos were incubated for 1 h with specific fluorescent secondary antibodies at room temperature after washing three times with washing buffer. Finally, the embryos were washed three times again followed by incubation with DAPI for 15 min, and then mounted on glass slides and examined with a laser scanning confocal microscope (Zeiss LSM 880 META, Germany). Z-series images were obtained to cover the maximal radius of individual nuclei and merged for each embryo. The foci in each picture were counted using Imaris 9.2.1 software. The parameters used for spot detection was estimated XY diameter, 0.4  $\mu$ m. Filter type was intensity sum of square. The analysis results were from at least three independent experiments. For protein location and  $\alpha$ -tubulin immunofluorescence staining in oocytes or embryos, pre-extraction was not needed and embryos were fixed first in 4% paraformaldehyde followed by permeabilization in membrane permeabilization solution (0.5% Triton X-100).

### BrdU staining

Two-cell embryos at different time points after one-cell division were incubated in KSOM medium supplemented with 100  $\mu$ M BrdU for 1 h. After incubation, the embryos were fixed for 20 min in 4% paraformaldehyde and permeabilized for 20 min in 0.5% Triton X-100. The embryos were then treated with 1.5 M HCl in PBS containing 1% Tween 20 for 7 min, and subsequently blocked in PBS containing 1 mg/ml BSA for 1 h at room temperature after washing three times with washing buffer. After blocking, the embryos were incubated overnight at 4°C with the anti-BrdU antibodies at appropriate dilutions, followed by staining with secondary Alexa Fluor FITC-conjugated antibody.

### Chromosome spread

Chromosome spreads were performed as previously described (Hodges and Hunt, 2002). Briefly, MII oocytes were collected and the zona pellucida was removed prior to fixation by transient exposure to Acid Tyrode's solution (Sigma-Aldrich). Zona-free oocytes were washed in M2 medium and then transferred onto a clean glass slide that was dipped in a solution of 1% paraformaldehyde in distilled H<sub>2</sub>O (pH 9.2) containing 0.15% Triton X-100

and 3 mM dithiothreitol. The slide dried slowly in a humid chamber for several hours and was stained with DAPI for analysis.

### Natural ovulation examination

For the natural ovulation assay, ~10-week-old female mice were mated with fertile males overnight. Successful mating was confirmed by the presence of vaginal plugs. Fertilized eggs were harvested from oviducts, counted and analyzed after removal of the cumulus mass by treatment with 3 mg/ml hyaluronidase (Sigma-Aldrich) in M2 medium.

### Culture and collection of mouse oocytes and early embryos

To harvest oocytes or embryos, females were intraperitoneally injected with 10 IU of PMSG followed by 10 IU of hCG after 48 h to promote ovulation. Oocytes or embryos were manipulated in M2 at the indicated time points after hCG injection: MII oocytes, 14 h; zygotes, 22–30 h; two-cell embryos, 48 h. Germinal vesicle stage (GV) oocytes were obtained 48 h after PMSG injection. The GV stage oocytes were isolated from ovaries and cultured in M2 medium under paraffin oil at 37°C, 5% CO<sub>2</sub> in air, while zygotes were cultured in KSOM medium. Oocytes and zygotes were collected at specific times of culture for immunofluorescence staining, western blotting or chromosome spread.

### Quantitative real-time RT-PCR

The mRNA was extracted from oocytes using RNeasy micro kit (Qiagen) according to the manufacturer's instructions. The first cDNA strand was synthesized using Superscript II (Invitrogen). Quantitative real-time PCR (qRT-PCR) was carried out using fast real-time PCR systems (ABI). Triple samples were analyzed for each gene, and the housekeeping gene *Gapdh* was used as control gene. The expression level was evaluated by  $2^{-\Delta\Delta Ct}$ . Primers are shown in Table S4.

### Comet assay of oocyte chromosome integrity

Oocytes harvested from ~10-week-old mice underwent a comet assay as previously described (Speit and Hartmann, 2006) with slight changes. In brief, oocytes were carefully blown into a 0.5% LMP (Low-melting-point) agarose layer that was covered by the normal melting agarose on a dish. The dish was incubated at 4°C for 5 min and then lowered into ice-cold freshly made lysing solution at 4°C for 1 h. The dish was then washed with distilled water three times and then the DNA was unwound using alkaline buffer for 20 min on ice. Electrophoresis was carried out at 25 V for 20 min. Finally, the cells on the dish were stained with ethidium bromide (20 µg/ml) for 15 min and then examined with a TE300 fluorescence microscope (Nikon, Japan). The comet tail length and comet tail DNA were analyzed using CASP software.

### Conventional western immunoblotting

A total of 200 oocytes or embryos were mixed with SDS sample buffer and boiled for 5 min at 100°C for SDS-PAGE. Western blot was performed as described previously (Qi et al., 2013), using antibodies against PPP4C, γH2AX, H2AX, p-CHK1<sup>S345</sup>, p-CDK1<sup>Y15</sup> and p-BRCA2<sup>S3291</sup> at 1:1000 and antibodies against GAPDH and α-tubulin at 1:2000. Suppliers and catalog codes are provided in Table S3.

### Automated western immunoblotting

The capillary-based western immunoblots were performed with sample prepared kit (Protein Simple) according to the manufacturer's standard instruction. Each sample, which included about 100 ng total protein of five embryos, was separated and detected on the WES System (Protein Simple). Proteins were detected with the following primary antibodies: rabbit anti-p-CHK2<sup>T68</sup>, rabbit anti-p-CHK2<sup>S383</sup>, rabbit anti-CHK2, rabbit anti-p-CDC25B<sup>S323</sup>, rabbit anti-CDC25B and rabbit anti-GAPDH. Suppliers and catalog codes are provided in Table S3.

### Nanoimmuno capillary isoelectric focusing

We performed Nanimmuno capillary isoelectric focusing (NICIF) with Nanopro 1000 (Protein Simple) following manufacturer's protocol. Briefly, each group of 30 embryos was washed once with Cell Wash Buffer and lysed

with 3 µl Bicine/CHAPS Lysis Buffer and Sample Diluent added 4× DMSO Inhibitor mix on ice for 30 min. Cell lysates were mixed with 9 µl Premix G2 pH3-10 separation gradient and loaded into a 384-well microplate. Anti-PLK1 antibody was diluted with Antibody Diluent at 1:50 and secondary antibody was diluted with Antibody Diluent at 1:100 (Table S3). The experiment was independently repeated twice. Data analysis was carried out using Compass Software.

### Construction of plasmids

Double-stranded DNA donor of mouse *ppp4c* was ordered from Sangon Biotech (Shanghai, China) and cloned into *puc57* vector. The *px330-ppp4c* sgRNA-L and *px330-ppp4c* sgRNA-R were used for expressing Cas9 and sgRNA *in vitro* transcription. Full-length mouse *ppp4c* was cloned into a *pcs2+* vector expressing MYC-tag and *plk1* was cloned into a *pcmv* vector expressing HA-tag. The gene *eGFP* was cloned from a *px458* vector and sub-cloned into the FseI-XbaI sites of *pcs2+*.

### mRNA microinjection of mouse zygotes

Full-length mouse *plk1* was cloned into modified *pcs2+* vector containing SP6 promoter. PCR-based *Plk1* point mutations were generated by mutating *Plk1* primers (Table S3) in the *pcs2+-plk1* vector using the KOD-Plus-Mutagenesis Kit (SMK-101, Toyobo). All plasmid constructs were verified by sequencing. Linearised plasmid was used for *in vitro* transcription with the mMESSAGE mMACHINE Kit (Ambion) and purified with an RNeasy MinElute Cleanup Kit (Qiagen). Purified mRNA concentrations were measured using UV spectrophotometer and then dissolved in nuclease-free water at 1200 ng/µl. Mouse zygotes at 24 h post-hCG were collected and microinjected with 5–10 pl mRNA and cultured in KSOM medium.

### Co-immunoprecipitation

293T cells were transfected with the indicated plasmids using Lipofectamine 3000 (L3000015, Invitrogen) according to the reagent protocol. At 40 h after transfection, cells were treated with 50 µg/ml etoposide or X-ray (10 Gy) to induce lesions. After 3 h, cells were collected and resuspended in lysis buffer (P0013, Beyotime) supplemented with protease inhibitor. Then, the lysates were incubated on ice for 30 min and centrifuged at 13,500 g for 15 min at 4°C. The supernatant was collected and 300 µl was incubated with 2 µl indicated antibody and 25 µl Protein A/G Magentic beads (B23201, bimake) for 6 h with rotation at 4°C. Beads were washed five times with lysis buffer, then 40 µl 1× SDS loading buffer was added for western blotting.

### Statistical analyses

All experiments were repeated at least three times. All analyses were performed using GraphPad Prism 5 software. Results are expressed as mean ± s.e.m. For all comparisons that involved multiple time points, a two-way repeated measurement ANOVA and post-hoc Bonferroni multiple-comparisons test were used to assess *P*-values. A two-tailed, unpaired Student's *t*-test was performed to compare two different groups, and an unpaired test was performed on non-parametric data. *P*<0.05 was considered statistically significant.

### Acknowledgements

We thank all members of the Sun lab for their help and discussions.

### Competing interests

The authors declare no competing or financial interests.

### Author contributions

Conceptualization: M.-Z.D., Q.-Y.S.; Methodology: M.-Z.D., Y.-C.O., X.-S.M.; Software: M.-Z.D.; Validation: Q.-Y.S.; Formal analysis: M.-Z.D., Q.-Y.S.; Investigation: M.-Z.D., S.-C.G.; Resources: Z.-B.W., Q.-Y.S.; Data curation: M.-Z.D.; Writing - original draft: M.-Z.D.; Writing - review & editing: H.S., Q.-Y.S.; Visualization: M.-Z.D.; Supervision: Z.-B.W., Q.-Y.S.; Project administration: Y.H., Z.-B.W., Q.-Y.S.; Funding acquisition: Q.-Y.S.

### Funding

This work was supported by the National Key Research and Development Program of China (2021YFA1100302), the National Natural Science Foundation of China (31530049) and by a Key Project of the Natural Science Foundation of Shandong Province, China (ZR2021ZD33).

## Peer review history

The peer review history is available online at <https://journals.biologists.com/dev/article-lookup/doi/10.1242/dev.200351>.

## References

- Anantha, R. W. and Borowiec, J. A. (2009). Mitotic crisis: the unmasking of a novel role for RPA. *Cell Cycle* **8**, 357-361. doi:10.4161/cc.8.3.7496
- Anantha, R. W., Sokolova, E. and Borowiec, J. A. (2008). RPA phosphorylation facilitates mitotic exit in response to mitotic DNA damage. *Proc. Natl. Acad. Sci. USA* **105**, 12903-12908. doi:10.1073/pnas.0803001105
- Artus, J. and Cohen-Tannoudji, M. (2008). Cell cycle regulation during early mouse embryogenesis. *Mol. Cell. Endocrinol.* **282**, 78-86. doi:10.1016/j.mce.2007.11.008
- Bohrer, R. C., Dicks, N., Gutierrez, K., Duggavathi, R. and Bordignon, V. (2018). Double-strand DNA breaks are mainly repaired by the homologous recombination pathway in early developing swine embryos. *FASEB J.* **32**, 1818-1829. doi:10.1096/fj.201700800R
- Buisson, R., Niraj, J., Rodrigue, A., Ho, C. K., Kreuzer, J., Foo, T. K., Hardy, E. J.-L., Delleire, G., Haas, W., Xia, B. et al. (2017). Coupling of homologous recombination and the checkpoint by ATR. *Mol. Cell* **65**, 336-346. doi:10.1016/j.molcel.2016.12.007
- Campos, A. and Clemente-Blanco, A. (2020). Cell cycle and DNA repair regulation in the damage response: protein phosphatases take over the reins. *Int. J. Mol. Sci.* **21**, 446. doi:10.3390/ijms21020446
- Chanut, P., Britton, S., Coates, J., Jackson, S. P. and Calsou, P. (2016). Coordinated nuclease activities counteract Ku at single-ended DNA double-strand breaks. *Nat. Commun.* **7**, 12889. doi:10.1038/ncomms12889
- Chapman, J. R., Taylor, M. R. G. and Boulton, S. J. (2012). Playing the end game: DNA double-strand break repair pathway choice. *Mol. Cell* **47**, 497-510. doi:10.1016/j.molcel.2012.07.029
- Chowdhury, D., Xu, X., Zhong, X., Ahmed, F., Zhong, J., Liao, J., Dykxhoorn, D. M., Weinstock, D. M., Pfeifer, G. P. and Lieberman, J. (2008). A PP4-phosphatase complex dephosphorylates  $\gamma$ -H2AX generated during DNA replication. *Mol. Cell* **31**, 33-46. doi:10.1016/j.molcel.2008.05.016
- Ciccia, A. and Elledge, S. J. (2010). The DNA damage response: making it safe to play with knives. *Mol. Cell* **40**, 179-204. doi:10.1016/j.molcel.2010.09.019
- Derijck, A., van der Heijden, G., Giele, M., Philippens, M. and de Boer, P. (2008). DNA double-strand break repair in parental chromatin of mouse zygotes, the first cell cycle as an origin of de novo mutation. *Hum. Mol. Genet.* **17**, 1922-1937. doi:10.1093/hmg/ddn090
- Elez, R., Piiper, A., Giannini, C. D., Brendel, M. and Zeuzem, S. (2000). Polo-like kinase1, a new target for antisense tumor therapy. *Biochem. Biophys. Res. Commun.* **269**, 352-356. doi:10.1006/bbrc.2000.2291
- Esashi, F., Christ, N., Gannon, J., Liu, Y., Hunt, T., Jasin, M. and West, S. C. (2005). CDK-dependent phosphorylation of BRCA2 as a regulatory mechanism for recombinational repair. *Nature* **434**, 598-604. doi:10.1038/nature03404
- Escribano-Díaz, C., Orthwein, A., Fradet-Turcotte, A., Xing, M., Young, J. T. F., Tkáč, J., Cook, M. A., Rosebrock, A. P., Munro, M., Canny, M. D. et al. (2013). A cell cycle-dependent regulatory circuit composed of 53BP1-RIF1 and BRCA1-CtIP controls DNA repair pathway choice. *Mol. Cell* **49**, 872-883. doi:10.1016/j.molcel.2013.01.001
- Ferretti, L. P., Lafranchi, L. and Sartori, A. A. (2013). Controlling DNA-end resection: a new task for CDKs. *Front Genet* **4**, 99. doi:10.3389/fgene.2013.00099
- Gebel, J., Tuppi, M., Sängler, N., Schumacher, B. and Dötsch, V. (2020). DNA damaged induced cell death in oocytes. *Molecules* **25**, 5714. doi:10.3390/molecules25235714
- Giunta, S., Belotserkovskaya, R. and Jackson, S. P. (2010). DNA damage signaling in response to double-strand breaks during mitosis. *J. Cell Biol.* **190**, 197-207. doi:10.1083/jcb.200911156
- He, D. C., Nickerson, J. A. and Penman, S. (1990). Core filaments of the nuclear matrix. *J. Cell Biol.* **110**, 569-580. doi:10.1083/jcb.110.3.569
- Hodges, C. A. and Hunt, P. A. (2002). Simultaneous analysis of chromosomes and chromosome-associated proteins in mammalian oocytes and embryos. *Chromosoma* **111**, 165-169. doi:10.1007/s00412-002-0195-3
- Huang, L., Meng, T.-G., Ma, X.-S., Wang, Z.-B., Qi, S.-T., Chen, Q., Zhang, Q.-H., Liang, Q.-X., Wang, Z.-W., Hu, M.-W. et al. (2019). Rad9a is involved in chromatin decondensation and post-zygotic embryo development in mice. *Cell Death Differ.* **26**, 969-980. doi:10.1038/s41418-018-0181-9
- Huertas, P. and Jackson, S. P. (2009). Human CtIP mediates cell cycle control of DNA end resection and double strand break repair. *J. Biol. Chem.* **284**, 9558-9565. doi:10.1074/jbc.M808906200
- Huertas, P., Cortés-Ledesma, F., Sartori, A. A., Aguilera, A. and Jackson, S. P. (2008). CDK targets Sae2 to control DNA-end resection and homologous recombination. *Nature* **455**, 689-692. doi:10.1038/nature07215
- Inoue, D. and Sagata, N. (2005). The Polo-like kinase Plx1 interacts with and inhibits Myt1 after fertilization of *Xenopus* eggs. *EMBO J.* **24**, 1057-1067. doi:10.1038/sj.emboj.7600567
- Isono, M., Niimi, A., Oike, T., Hagiwara, Y., Sato, H., Sekine, R., Yoshida, Y., Isobe, S.-Y., Obuse, C., Nishi, R. et al. (2017). BRCA1 directs the repair pathway to homologous recombination by promoting 53BP1 dephosphorylation. *Cell Rep.* **18**, 520-532. doi:10.1016/j.celrep.2016.12.042
- Jang, Y.-J., Ma, S., Terada, Y. and Erikson, R. L. (2002). Phosphorylation of threonine 210 and the role of serine 137 in the regulation of mammalian polo-like kinase. *J. Biol. Chem.* **277**, 44115-44120. doi:10.1074/jbc.M202172200
- Jang, Y.-J., Ji, J.-H., Choi, Y.-C., Ryu, C. J. and Ko, S.-Y. (2007). Regulation of Polo-like kinase 1 by DNA damage in mitosis. Inhibition of mitotic PLK-1 by protein phosphatase 2A. *J. Biol. Chem.* **282**, 2473-2482. doi:10.1074/jbc.M605480200
- Jazayeri, A., Falck, J., Lukas, C., Bartek, J., Smith, G. C. M., Lukas, J. and Jackson, S. P. (2006). ATM- and cell cycle-dependent regulation of ATR in response to DNA double-strand breaks. *Nat. Cell Biol.* **8**, 37-45. doi:10.1038/ncb1337
- Karlsson-Rosenthal, C. and Millar, J. B. A. (2006). Cdc25: mechanisms of checkpoint inhibition and recovery. *Trends Cell Biol.* **16**, 285-292. doi:10.1016/j.tcb.2006.04.002
- Keogh, M.-C., Kim, J.-A., Downey, M., Fillingham, J., Chowdhury, D., Harrison, J. C., Onishi, M., Datta, N., Galicia, S., Emili, A. et al. (2006). A phosphatase complex that dephosphorylates gammaH2AX regulates DNA damage checkpoint recovery. *Nature* **439**, 497-501. doi:10.1038/nature04384
- Khokhlova, E. V., Fesenko, Z. S., Sopova, J. V. and Leonova, E. I. (2020). Features of DNA repair in the early stages of mammalian embryonic development. *Genes (Basel)* **11**, 1138. doi:10.3390/genes11101138
- Lee, D.-H., Pan, Y., Kanner, S., Sung, P., Borowiec, J. A. and Chowdhury, D. (2010). A PP4 phosphatase complex dephosphorylates RPA2 to facilitate DNA repair via homologous recombination. *Nat. Struct. Mol. Biol.* **17**, 365-372. doi:10.1038/nsmb.1769
- Lee, D.-H., Goodarzi, A. A., Adelmant, G. O., Pan, Y., Jeggo, P. A., Marto, J. A. and Chowdhury, D. (2012). Phosphoproteomic analysis reveals that PP4 dephosphorylates KAP-1 impacting the DNA damage response. *EMBO J.* **31**, 2403-2415. doi:10.1038/emboj.2012.86
- Lee, D.-H., Acharya, S. S., Kwon, M., Drane, P., Guan, Y., Adelmant, G., Kalev, P., Shah, J., Pellman, D., Marto, J. A. et al. (2014). Dephosphorylation enables the recruitment of 53BP1 to double-strand DNA breaks. *Mol. Cell* **54**, 512-525. doi:10.1016/j.molcel.2014.03.020
- Lin, F., Ma, X.-S., Wang, Z.-B., Wang, Z.-W., Luo, Y.-B., Huang, L., Jiang, Z.-Z., Hu, M.-W., Schatten, H. and Sun, Q.-Y. (2014). Different fates of oocytes with DNA double-strand breaks in vitro and in vivo. *Cell Cycle* **13**, 2674-2680. doi:10.4161/15384101.2015.945375
- Lindahl, T. and Barnes, D. E. (2000). Repair of endogenous DNA damage. *Cold Spring Harb. Symp. Quant. Biol.* **65**, 127-134. doi:10.1101/sqb.2000.65.127
- Liu, Z., Sun, Q. and Wang, X. (2017). PLK1, a potential target for cancer therapy. *Transl. Oncol.* **10**, 22-32. doi:10.1016/j.tranon.2016.10.003
- Liu, J., Xu, L., Zhong, J., Liao, J., Li, J. and Xu, X. (2012). Protein phosphatase PP4 is involved in NHEJ-mediated repair of DNA double-strand breaks. *Cell Cycle* **11**, 2643-2649. doi:10.4161/cc.20957
- Lobjois, V., Jullien, D., Bouché, J.-P. and Ducommun, B. (2009). The polo-like kinase 1 regulates CDC25B-dependent mitosis entry. *Biochim. Biophys. Acta* **1793**, 462-468. doi:10.1016/j.bbamcr.2008.12.015
- Lowery, D. M., Lim, D. and Yaffe, M. B. (2005). Structure and function of Polo-like kinases. *Oncogene* **24**, 248-259. doi:10.1038/sj.onc.1208280
- Macůrek, L., Lindqvist, A., Lim, D., Lampson, M. A., Klompaker, R., Freire, R., Clouin, C., Taylor, S. S., Yaffe, M. B. and Medema, R. H. (2008). Polo-like kinase-1 is activated by aurora A to promote checkpoint recovery. *Nature* **455**, 119-123. doi:10.1038/nature07185
- Marangos, P. and Carroll, J. (2012). Oocytes progress beyond prophase in the presence of DNA damage. *Curr. Biol.* **22**, 989-994. doi:10.1016/j.cub.2012.03.063
- McManus, K. J. and Hendzel, M. J. (2005). ATM-dependent DNA damage-independent mitotic phosphorylation of H2AX in normally growing mammalian cells. *Mol. Biol. Cell* **16**, 5013-5025. doi:10.1091/mbc.e05-01-0065
- Mimitou, E. P. and Symington, L. S. (2010). Ku prevents Exo1 and Sgs1-dependent resection of DNA ends in the absence of a functional MRX complex or Sae2. *EMBO J.* **29**, 3358-3369. doi:10.1038/emboj.2010.193
- Murray, A. W. (2004). Recycling the cell cycle: cyclins revisited. *Cell* **116**, 221-234. doi:10.1016/S0092-8674(03)01080-8
- Nakada, S., Chen, G. I., Gingras, A. C. and Durocher, D. (2008). PP4 is a  $\gamma$ H2AX phosphatase required for recovery from the DNA damage checkpoint. *EMBO Rep.* **9**, 1019-1026. doi:10.1038/embo.2008.162
- Nakamura, K., Kustatscher, G., Alabert, C., Hödl, M., Forne, I., Völker-Albert, M., Satpathy, S., Beyer, T. E., Mailand, N., Choudhary, C. et al. (2021). Proteome dynamics at broken replication forks reveal a distinct ATM-directed repair response suppressing DNA double-strand break ubiquitination. *Mol. Cell* **81**, 1084-1099.e86. doi:10.1016/j.molcel.2020.12.025
- Nguyen, Q. N., Zerafa, N., Liew, S. H., Findlay, J. K., Hickey, M. and Hutt, K. J. (2019). Cisplatin- and cyclophosphamide-induced primordial follicle depletion is caused by direct damage to oocytes. *Mol. Hum. Reprod.* **25**, 433-444. doi:10.1093/molehr/gaz020
- Peng, B., Shi, R., Bian, J., Li, Y., Wang, P., Wang, H., Liao, J., Zhu, W.-G. and Xu, X. (2021). PARP1 and CHK1 coordinate PLK1 enzymatic activity during the DNA

- damage response to promote homologous recombination-mediated repair. *Nucleic Acids Res.* **49**, 7554-7570. doi:10.1093/nar/gkab584
- Qi, S.-T., Wang, Z.-B., Ouyang, Y.-C., Zhang, Q.-H., Hu, M.-W., Huang, X., Ge, Z., Guo, L., Wang, Y.-P., Hou, Y. et al. (2013). Overexpression of SET $\beta$ , a protein localizing to centromeres, causes precocious separation of chromatids during the first meiosis of mouse oocytes. *J. Cell Sci.* **126**, 1595-1603. doi:10.1242/jcs.116541
- Qian, Y.-W., Erikson, E., Taieb, F. E. and Maller, J. L. (2001). The polo-like kinase Plx1 is required for activation of the phosphatase Cdc25C and cyclin B-Cdc2 in *Xenopus* oocytes. *Mol. Biol. Cell* **12**, 1791-1799. doi:10.1091/mbc.12.6.1791
- San Filippo, J., Sung, P. and Klein, H. (2008). Mechanism of eukaryotic homologous recombination. *Annu. Rev. Biochem.* **77**, 229-257. doi:10.1146/annurev.biochem.77.061306.125255
- Sanchez, Y., Wong, C., Thoma, R. S., Richman, R., Wu, Z., Piwnica-Worms, H. and Elledge, S. J. (1997). Conservation of the Chk1 checkpoint pathway in mammals: linkage of DNA damage to Cdk regulation through Cdc25. *Science* **277**, 1497-1501. doi:10.1126/science.277.5331.1497
- Seki, A., Coppinger, J. A., Jang, C.-Y., Yates, J. R. and Fang, G. (2008). Bora and the kinase Aurora a cooperatively activate the kinase Plk1 and control mitotic entry. *Science* **320**, 1655-1658. doi:10.1126/science.1157425
- Shibata, A., Moiani, D., Arvai, A. S., Perry, J., Harding, S. M., Genoia, M.-M., Maity, R., van Rossum-Fikkert, S., Kertokallio, A., Romoli, F. et al. (2014). DNA double-strand break repair pathway choice is directed by distinct MRE11 nuclease activities. *Mol. Cell* **53**, 7-18. doi:10.1016/j.molcel.2013.11.003
- Smirnov, A., Fishman, V., Yunusova, A., Korablev, A., Serova, I., Skryabin, B. V., Rozhdestvensky, T. S. and Battulin, N. (2020). DNA barcoding reveals that injected transgenes are predominantly processed by homologous recombination in mouse zygote. *Nucleic Acids Res.* **48**, 719-735. doi:10.1093/nar/gkz1085
- Smits, V. A. J., Klompaker, R., Arnaud, L., Rijkse, G., Nigg, E. A. and Medema, R. H. (2000). Polo-like kinase-1 is a target of the DNA damage checkpoint. *Nat. Cell Biol.* **2**, 672-676. doi:10.1038/35023629
- Sørensen, C. S., Hansen, L. T., Dziegielewska, J., Syljuåsen, R. G., Lundin, C., Bartek, J. and Helleday, T. (2005). The cell-cycle checkpoint kinase Chk1 is required for mammalian homologous recombination repair. *Nat. Cell Biol.* **7**, 195-201. doi:10.1038/ncb1212
- Speit, G. and Hartmann, A. (2006). The comet assay: a sensitive genotoxicity test for the detection of DNA damage and repair. *Methods Mol. Biol.* **314**, 275-286. doi:10.1385/1-59259-973-7.275
- Syljuåsen, R. G., Jensen, S., Bartek, J. and Lukas, J. (2006). Adaptation to the ionizing radiation-induced G2 checkpoint occurs in human cells and depends on checkpoint kinase 1 and Polo-like kinase 1 kinases. *Cancer Res.* **66**, 10253-10257. doi:10.1158/0008-5472.CAN-06-2144
- Symington, L. S. and Gautier, J. (2011). Double-strand break end resection and repair pathway choice. *Annu. Rev. Genet.* **45**, 247-271. doi:10.1146/annurev-genet-110410-132435
- Tang, J., Erikson, R. L. and Liu, X. (2006). Checkpoint kinase 1 (Chk1) is required for mitotic progression through negative regulation of polo-like kinase 1 (Plk1). *Proc. Natl. Acad. Sci. USA* **103**, 11964-11969. doi:10.1073/pnas.0604987103
- Tang, Q., Li, W., Zheng, X., Ren, L., Liu, J., Li, S., Wang, J. and Du, G. (2020). MELK is an oncogenic kinase essential for metastasis, mitotic progression, and programmed death in lung carcinoma. *Signal Transduct. Target Ther.* **5**, 279. doi:10.1038/s41392-020-00288-3
- Toyo-oka, K., Mori, D., Yano, Y., Shiota, M., Iwao, H., Goto, H., Inagaki, M., Hiraiwa, N., Muramatsu, M., Wynshaw-Boris, A. et al. (2008). Protein phosphatase 4 catalytic subunit regulates Cdk1 activity and microtubule organization via NDEL1 dephosphorylation. *J. Cell Biol.* **180**, 1133-1147. doi:10.1083/jcb.200705148
- Trovesi, C., Manfrini, N., Falcattoni, M. and Longhese, M. P. (2013). Regulation of the DNA damage response by cyclin-dependent kinases. *J. Mol. Biol.* **425**, 4756-4766. doi:10.1016/j.jmb.2013.04.013
- van Vugt, M. A. T. M., Brás, A. and Medema, R. H. (2004). Polo-like kinase-1 controls recovery from a G2 DNA damage-induced arrest in mammalian cells. *Mol. Cell* **15**, 799-811. doi:10.1016/j.molcel.2004.07.015
- van Vugt, M. A. T. M., Gardino, A. K., Linding, R., Ostheimer, G. J., Reinhardt, H. C., Ong, S.-E., Tan, C. S., Miao, H., Keezer, S. M., Li, J. et al. (2010). A mitotic phosphorylation feedback network connects Cdk1, Plk1, 53BP1, and Chk2 to inactivate the G(2)/M DNA damage checkpoint. *PLoS Biol.* **8**, e1000287. doi:10.1371/journal.pbio.1000287
- Wang, H., Shi, L. Z., Wong, C. C. L., Han, X., Hwang, P. Y.-H., Truong, L. N., Zhu, Q., Shao, Z., Chen, D. J., Berns, M. W. et al. (2013). The interaction of CtIP and Nbs1 connects CDK and ATM to regulate HR-mediated double-strand break repair. *PLoS Genet.* **9**, e1003277. doi:10.1371/journal.pgen.1003277
- Wang, H., Qiu, Z., Liu, B., Wu, Y., Ren, J., Liu, Y., Zhao, Y., Wang, Y., Hao, S., Li, Z. et al. (2018). PLK1 targets CtIP to promote microhomology-mediated end joining. *Nucleic Acids Res.* **46**, 10724-10739. doi:10.1093/nar/gky810
- West, S. C. (2003). Molecular views of recombination proteins and their control. *Nat. Rev. Mol. Cell Biol.* **4**, 435-445. doi:10.1038/nrm1127
- Xu, Q., Wang, F., Xiang, Y., Zhang, X., Zhao, Z.-A., Gao, Z., Liu, W., Lu, X., Liu, Y., Yu, X.-J. et al. (2015). Maternal BCAS2 protects genomic integrity in mouse early embryonic development. *Development* **142**, 3943-3953. doi:10.1242/dev.129841
- Yata, K., Lloyd, J., Maslen, S., Bleuyard, J.-Y., Skehel, M., Smerdon, S. J. and Esashi, F. (2012). Plk1 and CK2 act in concert to regulate Rad51 during DNA double strand break repair. *Mol. Cell* **45**, 371-383. doi:10.1016/j.molcel.2011.12.028
- Yoo, H. Y., Kumagai, A., Shevchenko, A., Shevchenko, A. and Dunphy, W. G. (2004). Adaptation of a DNA replication checkpoint response depends upon inactivation of Claspin by the Polo-like kinase. *Cell* **117**, 575-588. doi:10.1016/S0092-8674(04)00417-9
- Yuan, J. H., Feng, Y., Fisher, R. H., Maloid, S., Longo, D. L. and Ferris, D. K. (2004). Polo-like kinase 1 inactivation following mitotic DNA damaging treatments is independent of ataxia telangiectasia mutated kinase. *Mol. Cancer Res.* **2**, 417-426.
- Zhang, C.-Z., Spektor, A., Cornils, H., Francis, J. M., Jackson, E. K., Liu, S., Meyerson, M. and Pellman, D. (2015). Chromothripsis from DNA damage in micronuclei. *Nature* **522**, 179-184. doi:10.1038/nature14493
- Zhang, W., Chen, Z., Zhang, D., Zhao, B., Liu, L., Xie, Z., Yao, Y. and Zheng, P. (2019). KHD3L mutation causes recurrent pregnancy loss by inducing genomic instability of human early embryonic cells. *PLoS Biol.* **17**, e3000468. doi:10.1371/journal.pbio.3000468

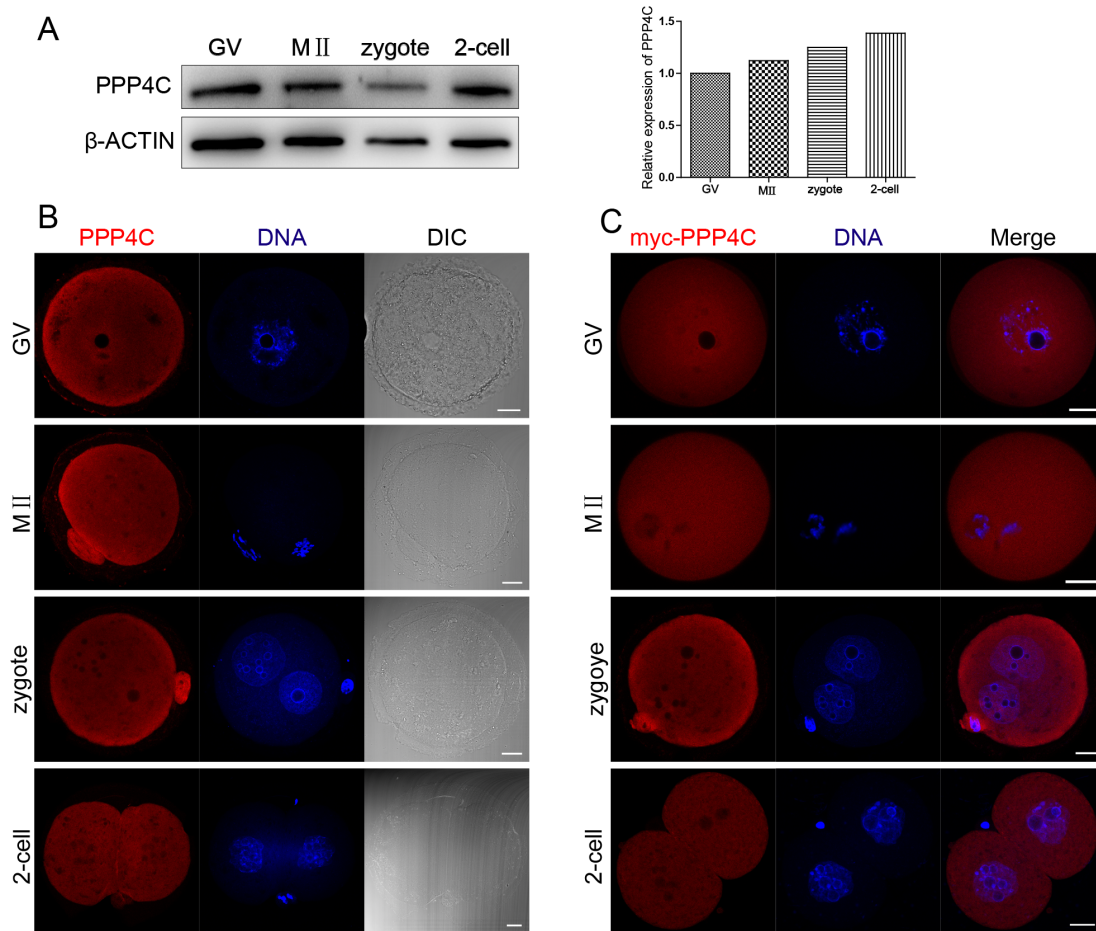


**Fig. S1. Characterization of PPP4C during mouse oocyte meiotic maturation and early embryo development.** (A) Western blot showing the expression pattern of PPP4C in oocytes, zygotes and 2-cell embryos. A total of 100 oocytes were collected after being cultured for 0 and 14 h, corresponding to the germinal vesicle (GV) and metaphase II (MII) stages, respectively. A total of 100 embryos were collected at 24 h and 48h after hCG treatment with successful mating, corresponding to 1-cell and 2-cell stages. Samples were immunoblotted using anti-PPP4C and anti- $\beta$ -ACTIN antibodies. (B) Representative images of subcellular localization of PPP4C during oocyte meiotic maturation and early embryo development. Oocytes were double stained for PPP4C (red) and DNA (blue) at the GV, MII, 1-cell and 2-cell stages. (C) Representative images of subcellular localization of myc-PPP4C during oocyte meiotic maturation and early embryo development. Cells were injected with *myc-Ppp4c* mRNA before staining. Scale bars: 20  $\mu$ m.



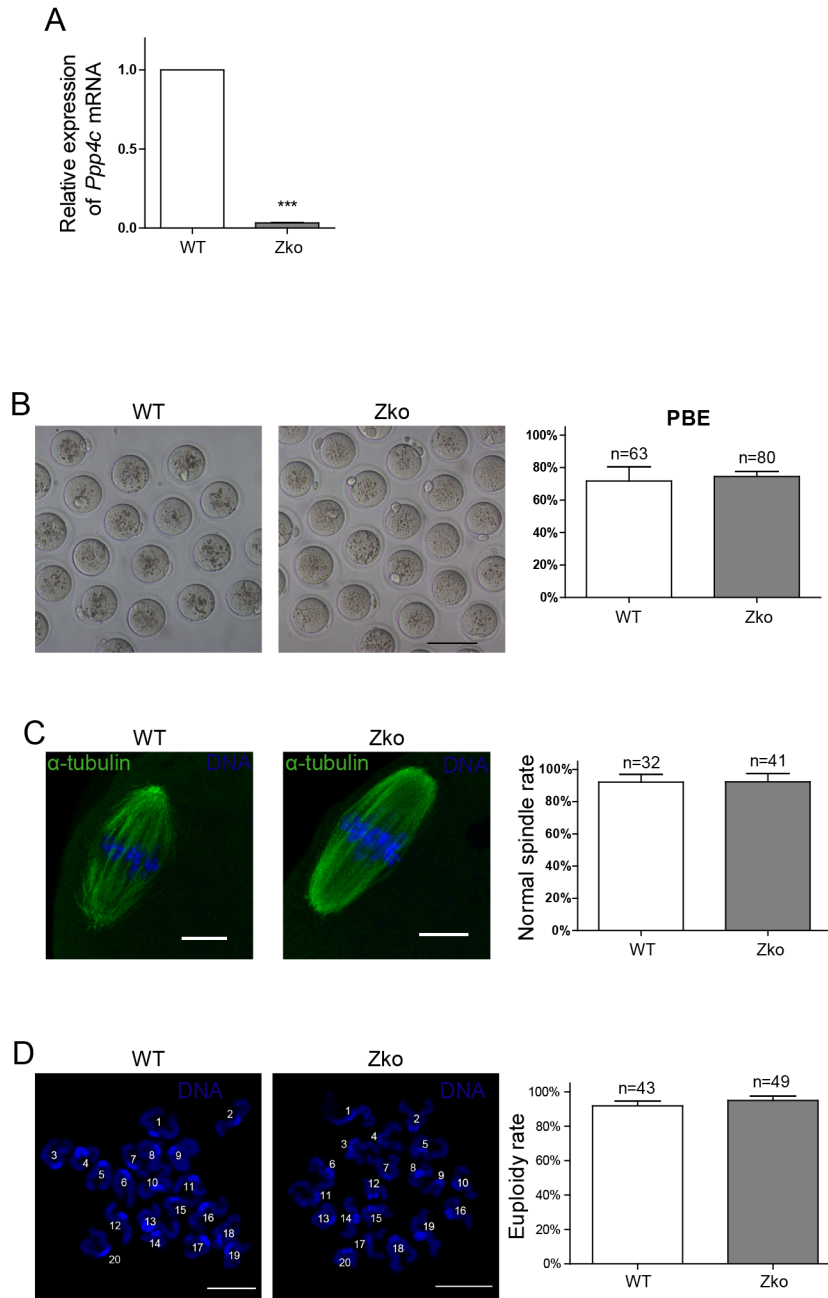


**Fig. S2. Depletion of PPP4C does not affect oocyte meiotic maturation.** (A) Total RNA samples prepared with ~50 WT and Zko oocytes and subjected to real-time RT-PCR showed no expression of *Ppp4c* mRNA in Zko oocytes. Results are mean  $\pm$  SEM. \* \* \* $P < 0.001$ . (B) Comparable PBE rates of WT and Zko oocytes. Germinal vesicle (GV) oocytes were isolated and matured in vitro; oocytes that extruded the first polar body (PBE) were counted at 14 h. Representative DIC images are shown. Data are presented

as mean  $\pm$  SEM. In vitro maturation (IVM) experiments were repeated at least three times. Scale bars: 100  $\mu$  m. (C) Representative images of staining for DNA (blue) and immunostaining for  $\alpha$ -tubulin (green) showing normal spindle assembly in Zko oocytes at the metaphase of M II stage. Scale bars: 10  $\mu$  m. The percentages of oocytes with a normal spindle at the M II stage of each genotype are presented as mean  $\pm$  SEM. The numbers of analyzed oocytes are indicated (n). (D) Chromosome spread of M II oocytes from WT and Zko mice, showing chromosomes stained with DAPI (blue). Representative images are shown. Scale bars: 10  $\mu$  m. The number of chromosomes from each oocyte was counted and the percentages showing euploidy (i.e. 20 pairs of chromatids) M II oocytes of each genotype are presented as mean  $\pm$  SEM. The total numbers of analyzed oocytes are indicated (n).

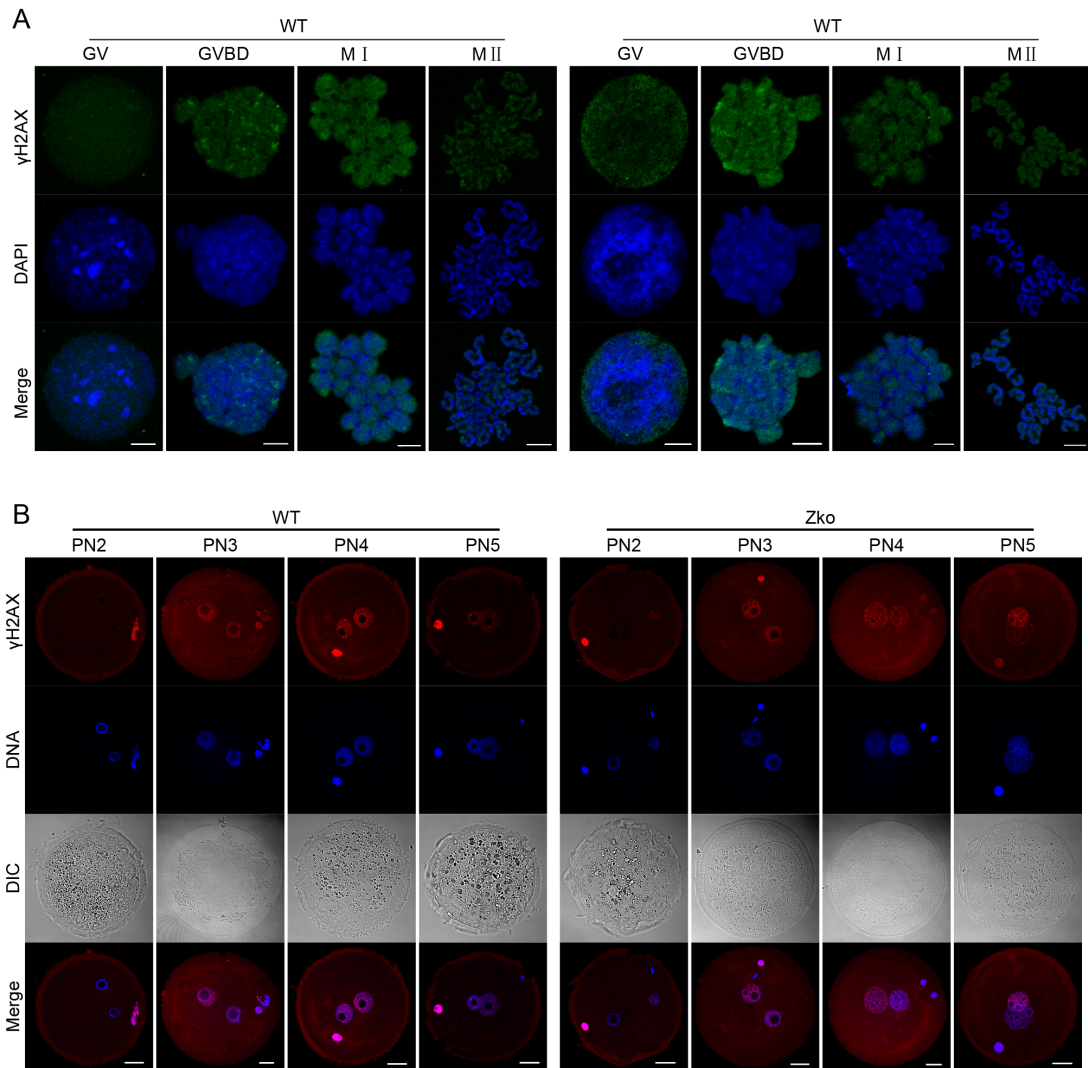


**Fig. S3. Depletion of PPP4C impairs genomic integrity of fertilized eggs.** (A)  $\gamma$  H2AX was assessed during oocyte maturation using chromatin spread preparations (B) Zygotes of WT and Zko females were obtained at 22, 24, 28 and 30 h post-hCG and stained with anti- $\gamma$ H2AX antibody. Scale bars: 20  $\mu$ m.

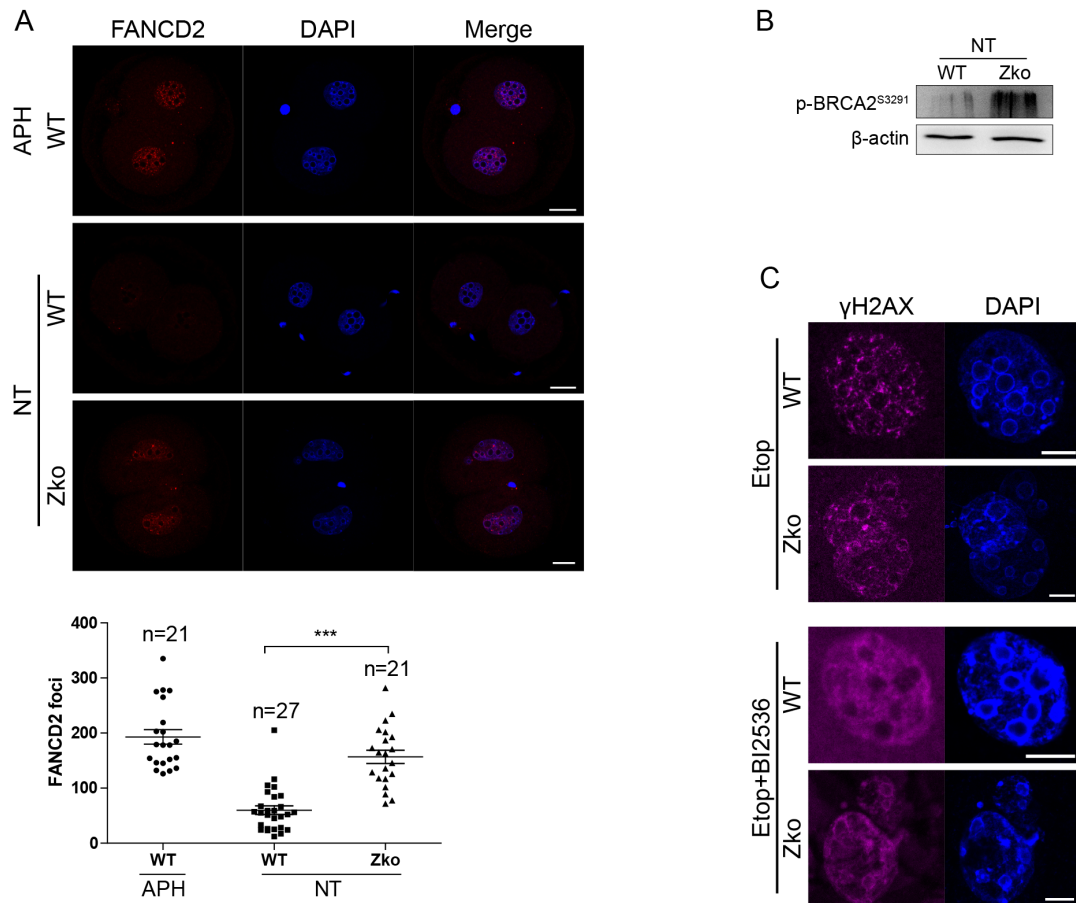


**Fig. S4.** (A) FANCD2 foci were assessed in G2 phase 2-cell WT and Zko embryos. Aphidicolin (an inhibitor of DNA synthesis, APH, 0.1  $\mu$ g/mL treated from G1 to G2 phase) treated group was used as a positive control. Foci were analyzed with imaris software. Results are mean  $\pm$  SEM from three independent experiments. \* \* \*P < 0.001. The total numbers of analyzed embryos are indicated as n. (B) BRCA2 S3291 was hyperphosphorylation in PPP4C-deficiency 2-cell embryos. Levels of the indicated proteins in G2 phase of 2-cell embryos were analyzed by Western blot. (C) Inhibition of PLK1 since G1 phase affects  $\gamma$  H2AX foci. 2-cell embryos were treated with or without BI2536 since G1 phase, and DNA damage was induced by etoposide for 3h in G2 phase before staining.

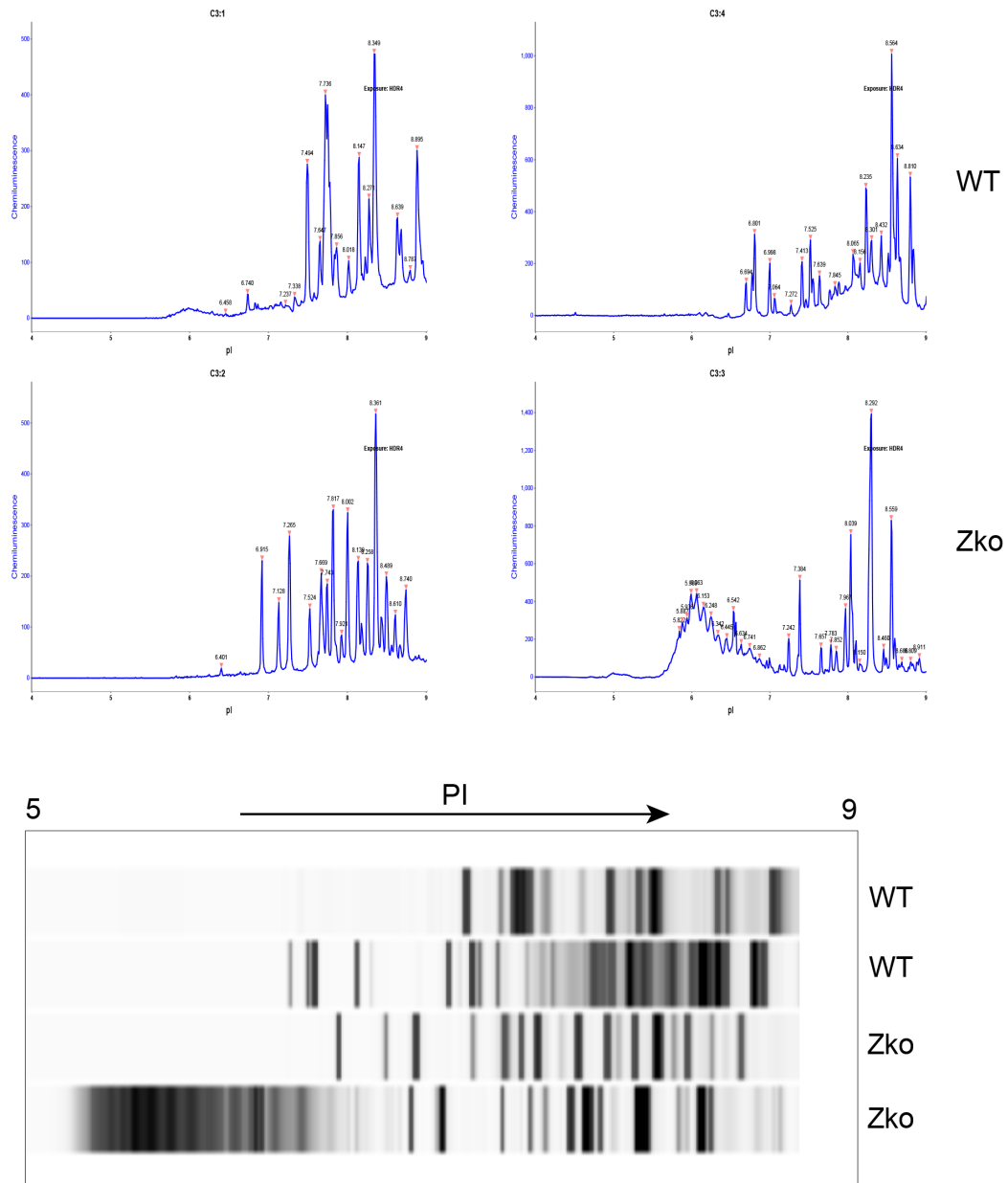


**Fig. S5. Quantification of posttranslational modification (PTM) of PLK1 in G2 phase of 2-cell embryos as revealed by NICIF.** Top, representative traces for PLK1. Bottom, NICIF pseudoblots representation.

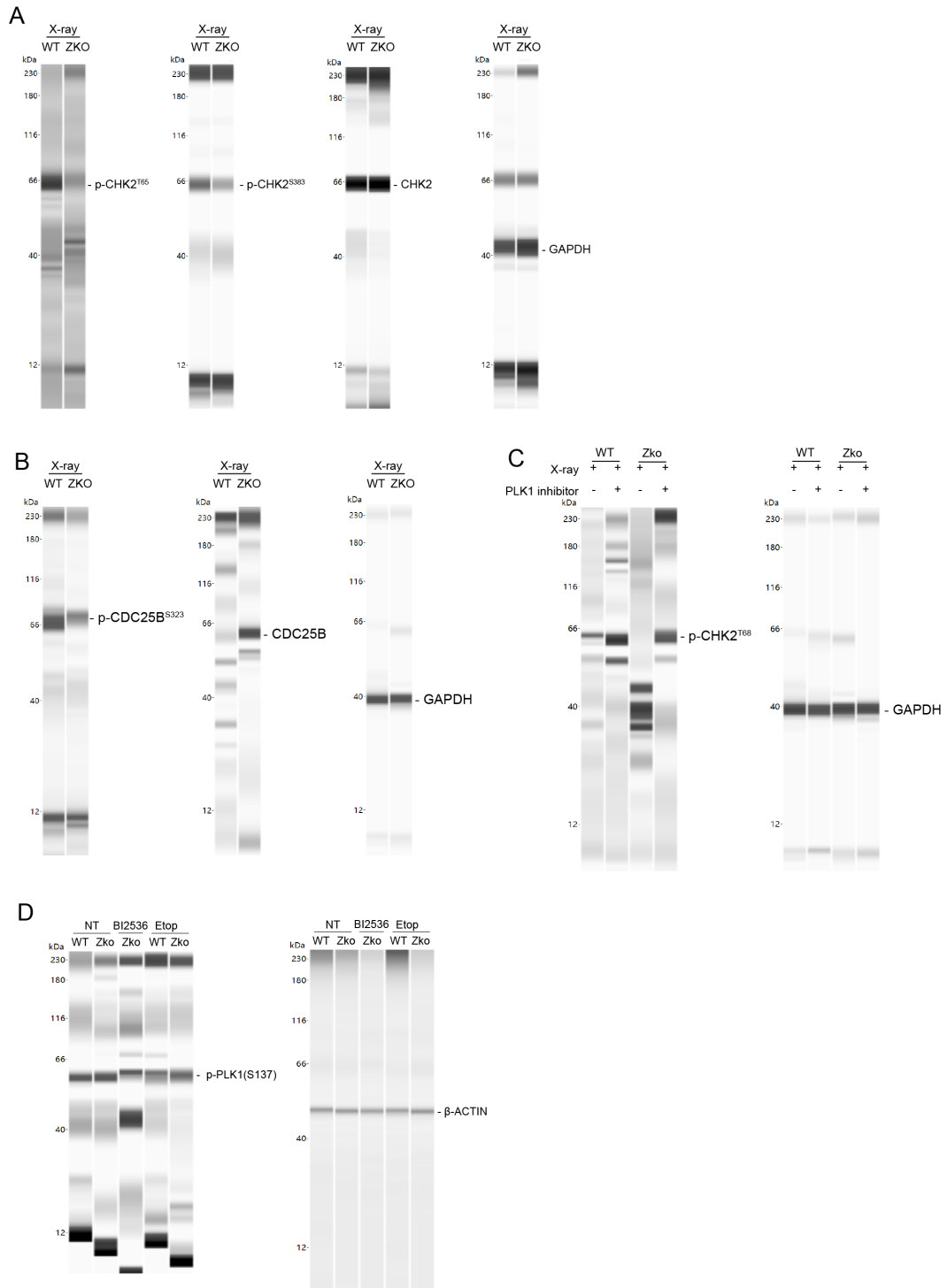


Fig. S6. Entire original wes pictures.

**Table S1. Original data of breeding assay.**

	WT				Zko			
	F2710	F7253	F7037	F5386	F2708	F2797	F7255	F7040
1st mon	4	9	5	7	0	0	3	0
2nd mon	11	15	11	12	4	0	13	3
3rd mon	19	15	16	21	4	4	20	6
4th mon	25	27	22	28	4	4	20	6
5th mon	30	31	35	30	8	7	25	10
6th mon	36	40	45	30	8	7	25	17
litters/mother	7	5	6	5	2	2	4	4

**Table S2. Original data of embryos at E10.5.**

	NO. embryos/female							
WT	8	9	9	7	4	8	8	10
Zko	2	5	4	5	1	5	7	6

**Table S3. Antibodies and reagents.**

Name	Application	Dilution
anti-PPP4C(Abcam,ab16475)	IF	1:200
	WB	1:1000
anti-RAD51 (Abcam,ab133534)	IF	1:200
anti-BrdU (Abcam,ab6326)	IF	1:200
anti- $\alpha$ -tubulin (Sigma,DM1A)	IF	1:1000
PLK1 (Sigma,SAB1404220)	WB	1:1000
	NICIF	1:50
anti-MYC (Sigma,M4439)	IF	1:1000
anti- $\gamma$ H2AX (Cell Signaling,5438S)	IF	1:200
	WB	1:1000
anti- $\gamma$ H2AX (Cell Signaling,7631T)	IF	1:200
	WB	1:1000
anti-p-CHK1 <sup>S345</sup> (Cell Signaling,2341S)	WB	1:1000
anti-RPA2 (Cell Signaling,2208)	IF	1:200
anti-GAPDH (Cell Signaling,5174)	WB	1:1000
	Wes	1:100
anti- $\alpha$ -tubulin(Cell Signaling,2144)	WB	1:1000
anti-p-CDK1 Y15 (Abclonal,AP0016)	WB	1:1000
anti-HA (Abclonal, AE008)	WB	1:1000
	IP	1:25
anti-CHK2 (Abclonal,A0466)	Wes	1:25
anti-p-BRCA2 <sup>S3291</sup> (Immunoway,YP0512)	WB	1:1000

anti-p-CHK2 <sup>T68</sup> (Immunoway, YP0065)	Wes	1:25
anti-p-CHK2 <sup>S383</sup> (Immunoway, YP0538)	Wes	1:25
anti-p-CDC25B <sup>S323</sup> (Immunoway, YP0057)	Wes	1:25
anti-p-PLK1 <sup>T210</sup> (Immunoway, YP0964)	WB	1:1000
anti-p-PLK1 <sup>S137</sup> (Immunoway, YP0434)	Wes	1:25
anti-FANCD2 (Abcam, ab108928)	IF	1:200
alexa 594 goat anti-rabbit (Invitrogen, A11012)	IF	1:1000
alexa FITC goat anti-rat (ZSGB-Bio, ZF-0315)	IF	1:1000
alexa 488 goat anti-mouse (Invitrogen, A11029)	IF	1:1000
alexa 647 goat anti-mouse (Invitrogen, A31571)	IF	1:1000
HRP-conjugated anti-mouse (ZSGB-BIO, 2304)	WB	1:2000
HRP-conjugated anti-rabbit (ZSGB-BIO, 2301)	WB	1:2000
Ro-3306 (selleck, s7747)	CDK1 inhibitor	10 $\mu$ M
BI-2536 (Medchemexpress, HY-50698)	Plk1 inhibitor	200nM
BML-277 (selleck, S8632)	CHK2 inhibitor	10 $\mu$ M
Etoposide (Sigma, E1383)	lesion inducer	50ug/ml
BrdU (Sigma, 858811)	DNA synthesis maker	100uM
aphidicolin (Sigma, A-0781)	DNA synthesis inhibitor	0.1ug/ml

Abbreviation:

IF, immunofluorescence staining

NICIF, Nanimmuno capillary isoelectric focusing

WB, western blotting

Wes, Automated Western immunoblotting

**Table S4. Primer sequences.**

	Name	5'->3'
Guiding RNA targeting at Ppp4c	sgRNA-L	CACCGGTCAGGAATTGGGCTGGGC
		AAACGCCAGCCCAATTCCTGACC
	sgRNA-R	CACCGCCTCGATACAAGAATTAGA
		AAACTCTAATTCTTGTATCGAGGC
PCR	Ppp4c-detF	GCATACTTCTGTCCCACG
	Ppp4c-detR	GTGTTTCCTGGGAGACTCCC
qRT-PCR	Ppp4c-qF	CTTGGTAGAAGAGAGCAACGTG
	Ppp4c-qR	CGCCACCTACTCTGAACAGC
	Gapdh-qF	TTGTCTCCTGCGACTTCAACA
	Gapdh-qR	ACCAGGAAATGAGCTTGACAAAG
Site-directed mutant	PLK1-S137D-F	GACCTCCTGGAGCTGCACA
	PLK1-S137A-F	GCCCTCCTGGAGCTGCAC
	PLK1-S137-R	CCTCCTGCGACAGAGCTC
	PLK1-T210D-F	GACTTGTGTGGCACTCCTA
	PLK1-T210A-F	GCCTTGTGTGGCACTCCT
	PLK1-T210-R	CTTCTTTCGTTCCCCTTCATAT